JPhys Photonics

TOPICAL REVIEW • OPEN ACCESS

Ultrafast adiabatic frequency conversion

To cite this article: Peleg Margules *et al* 2021 *J. Phys. Photonics* **3** 022011

View the article online for updates and enhancements.

This content was downloaded from IP address 68.175.138.86 on 09/04/2021 at 17:40

Journal of Physics: Photonics

OPEN ACCESS

RECEIVED
3 April 2020

REVISED
16 July 2020

ACCEPTED FOR PUBLICATION
10 January 2021

PUBLISHED
8 April 2021

Original content from this work may be used under the terms of the Creative Commons Attribution 4.0 licence.

Any further distribution of this work must maintain attribution to the author(s) and the title of the work, journal citation and DOI.

TOPICAL REVIEW

Ultrafast adiabatic frequency conversion

Peleg Margules[1], Jeffrey Moses[2], Haim Suchowski[1] and Gil Porat[3]

[1] Raymond and Beverly Sackler School of Physics and Astronomy, Tel Aviv University, 69978 Tel Aviv, Israel
[2] School of Applied and Engineering Physics, Cornell University, Ithaca, NY 14853, United States of America
[3] Department of Electrical and Computer Engineering, University of Alberta, Edmonton, Alberta T6G 1H9, Canada

E-mail: gporat@ualberta.ca

Keywords: ultrafast physics, frequency conversion, adiabatic evolution, nonlinear optics, attosecond dynamics

Abstract

Ultrafast adiabatic frequency conversion is a powerful method, capable of efficiently and coherently transfering ultrashort pulses between different spectral ranges, e.g. from near-infrared to mid-infrared, visible or ultra-violet. This is highly desirable in research fields that are currently limited by available ultrafast laser sources, e.g. attosecond science, strong-field physics, high-harmonic generation spectroscopy and multidimensional mid-infrared spectroscopy. Over the past decade, adiabatic frequency conversion has substantially evolved. Initially applied to quasi-monochromatic, undepleted pump interactions, it has been generalized to include ultrashort, broadband, fully-nonlinear dynamics. Through significant theoretical development and experimental demonstrations, it has delivered new capabilities and superior performance in terms of bandwidth, efficiency and robustness, as compared to other frequency conversion techniques. This article introduces the concept of adiabatic nonlinear frequency conversion, reviews its theoretical foundations, presents significant milestones and highlights contemporary ultrafast applications that may, or already do, benefit from utilizing this method.

1. Introduction

Ultrafast sources are at the heart of research breakthroughs in many fields, ranging from strong-field light-matter interactions and multi-photon spectroscopies, to communication, sensing and more. Tremendous progress has been achieved in the past few decades towards realizing high power, high energy, broadband, ultrashort-pulse coherent sources. However, there are wide frequency ranges where such sources are not available via direct laser action, or fall short of the requirements of applications, e.g. mid-IR. Nonlinear frequency conversion is a powerful solution to the absence of adequate lasers, allowing highly-efficient and coherent transfer of properties of excellent laser sources from one part of the spectrum to another.

Progress in attosecond science is strongly linked to progress in ultrafast laser technology. Ultrafast laser sources are critical tools that can be used to directly resolve attosecond dynamics in strong-field phenomena, or generate attosecond pulses that can probe physical phenomena on this time scale [1, 2]. Over the past three decades, much of the work in the field has been carried out using Ti:Sapphire laser systems. These laser systems provide the necessary pulse energy (usually >1 mJ) and short pulse duration (commonly <40 fs) in the near-IR spectral region. However, access to such sources in other spectral ranges, especially in the mid-IR, is highly desirable [3–5].

First, the fundamental dynamics of strong-field phenomena depend strongly on the driving field's wavelength, as tunnel-ionized electron trajectories are shaped by the field. Consequently, the manner in which these photoelectrons recombine with, or scatter off, parent atoms and molecules depends drastically on the field's wavelength. In particular, the ponderomotive energy acquired by the photoelectrons scales as the square of the driving laser wavelength [1, 2], thus scaling of up to 20-fold is offered by ultrafast laser sources at mid-IR wavelengths. As the spectral range of ultrafast sources available for such experiments expands, new regimes of attosecond physical phenomena can be explored.

© 2021 The Author(s). Published by IOP Publishing Ltd

Wavelength scaling of the photoelectron scattering process can be used to probe molecular structure over wide spatial and temporal ranges [6]. Another approach is high-harmonic generation (HHG) spectroscopy, which utilizes photoelectron recombination to probe attosecond-scale dynamics [7]. There is strong interest in extending this method to large and biologically-relevant molecules [8]. However, most biomolecules have low ionization potential, which leads to ionization saturation that prevents the useful application of HHG spectroscopy. The lower photon energy associated with mid-infrared light as compared to near-infrared light can address this challenge.

Second, as the generation of attosecond pulses itself is driven by ultrafast lasers, extending the spectral reach of these lasers directly translates into the extension of the spectral reach of attosecond pulses. In HHG, a decrease of the driving frequency results in an increase of the highest generated frequency (cut-off frequency), due to the ponderomotive energy scaling. Another approach utilizes a short-wavelength source to ionize an atom and subsequently drive HHG in the ion. Since the cut-off frequency also depends on the ionization potential, this ion HHG yields much higher frequencies. Both approaches reach into the x-ray spectral range [9, 10]. Each development of an attosecond pulse source in a new spectral range opens a window into atomic, molecular and material systems and phenomena that previously could not be probed on this time scale.

Fully-controllable broadband (multi-octave) ultrafast mid-IR sources are also of great importance in materials science, chemistry, biology and condensed-matter physics: the fundamental vibrational modes of many solids and biologically-significant molecules are in the mid-IR. Ultrafast mid-IR laser sources have been extensively utilized for resolving the femtosecond-scale dynamics in such physical systems, e.g. via multidimensional spectroscopy [11] or coherent control of lattice displacement [12]. As in attosecond science, achieving arbitrary shaping of few-cycle mid-IR pulses will provide control over coherent dynamics of material systems. This control will make it possible to follow energy flow between internal states of materials, with new levels of temporal resolution and state-distinguishability (via improved spectral resolution) [13].

The work toward such novel laser technology faces challenges on a number of fronts, where technical progress would translate directly to scientific advances. In the context of attosecond science [14], these include limited attosecond pulse flux, temporal-shape tailoring of driving mid-IR pulses and high-energy mid-IR sources for generating attosecond pulses in the x-ray spectral range. In a broader context of ultrafast mid-IR sources, arbitrary pulse-shaping of few-cycle (multi-octave) pulses remains a significant technical challenge. One might try to shape a near-IR pulse and use it to drive mid-IR generation. However, commonly used nonlinear methods for generating broadband mid-IR (e.g. supercontinuum generation) couple intensity and phase or need a (not-shaped) short driving pulse. Therefore, they cannot transfer the near-IR driver's pulse-shape to the generated mid-IR pulse. Direct shaping of the generated mid-IR over multiple spectral octaves is also very challenging, as there is no appropriate optical actuator (e.g. spatial light modulator, SLM) that covers the entire spectral range of interest to vibrational spectroscopy (2.5–20 μm). Single-cycle pulses have been successfully shaped with methods that address each part of the spectrum separately followed by coherent combining [15–17], however at the cost of great experimental complexity.

One approach that could address these issues is optical frequency conversion. In optical frequency conversion, energy is coherently transferred between optical waves at different frequencies. The interaction between these waves is mediated by a nonlinear medium in which they propagate. Most commonly, the goal is to transfer as much energy as possible from one spectral range to another. Frequency conversion processes have an inherent challenge. Due to the dispersive nature of matter, the driving and generated waves travel through the nonlinear medium at different phase velocities. This phase-mismatch severely diminishes the conversion efficiency [18]. Multiple techniques (reviewed below) have been developed to compensate for the phase-mismatch. Each technique has different strengths and weaknesses; however, many share a common thread: a trade-off between efficiency and robustness to variation in parameters such as temperature and wavelength. The latter strongly restricts the application of frequency conversion of ultrafast lasers, which are broadband by their nature.

Over the past decade, ultrafast adiabatic frequency conversion has emerged as a method that can address all these challenges. It facilitates efficient, broadband and coherent frequency conversion. In this manner, it effectively transfers the capabilities of highly developed pulse-shaping tools from the near-IR to other parts of the spectrum.

Unique challenges in ultrafast frequency conversion rise due to the inherently broad spectrum, which is acutely influenced by the dispersion of the materials in which pulses propagate. Group velocity mismatch (GVM), group velocity dispersion (GVD) and further high-order dispersion, cause a temporal walk-off between the interacting waves and cause the pulses to spread, reducing the overall efficiency of the interaction.

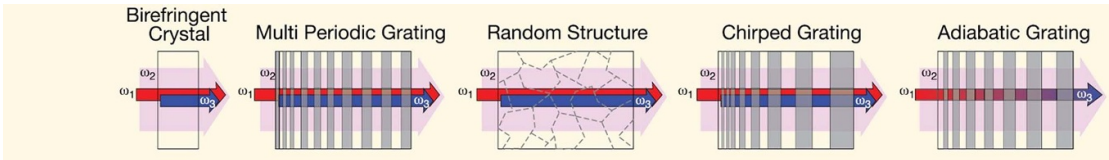

	Birefringent Crystal	Multi Periodic Grating	Random Structure	Chirped Grating	Adiabatic Grating
Bandwidth	Moderate	Narrow	Very wide	Wide	Wide
Efficiency	Low	High	Very low	Low to moderate	Very high
Cost and complextiy	Very low	High	Low	High	Very high
Preservation of spectrum	No	No	Yes	Yes	Yes

Figure 1. Comparison of broadband frequency conversion techniques. Reprinted with permission from [21].

In this review article we cover both the theoretical foundations of the adiabatic frequency conversion technique along with various examples of experimental realizations, with a special emphasis on ultrafast optics applications. The adiabatic technique has proved to be extremely valuable owing to its ability to overcome the efficiency-bandwidth trade-off. In recent years, both theory and experiments have expanded this method to include a broad operational space of ultrafast nonlinear optics.

While much of the work done so far has focused on demonstrating efficient broadband frequency conversion, several works have demonstrated the potential of the method to allow the flexible temporal shaping of energetic and broadband—even greater than octave spanning—pulses, allowing precise control of the temporal pulse shape. These include: (a) programmable pulse shaping of energetic mid-IR pulses spanning 1.3 octaves [19]. Single-cycle pulses were obtained, as well as the ability to impress complex pulse shapes, such as the modulation required to generate single-cycle pulse pairs with arbitrary temporal separation (discussed in section 2.5); (b) spectral phase shaping in adiabatic second harmonic generation (SHG) allows for the creation of complex temporal pulse shapes when frequency doubling sub-100 fs pulses [20] (discussed in section 4); (c) adiabatic downconversion by four-wave mixing (FWM) in hollow optical fiber that preserves the pulse phase, allowing pre-conversion pulse shaping that can simplify dispersion management for a very broadband pulse and that is independent of the pulse energy. The same method could be used to generate high-energy pulses with a passively stabilized CEP in the near-octave-spanning down-converted pulse (discussed in section 6). While these pulse conversion technologies have not yet been used for attosecond pulse generation and the control of other strong-field phenomena, these preliminary works that have investigated and/or demonstrated efficient, ultrabroadband bandwidth conversion combined with the capability for precise control of the generated time-domain pulse characteristics, demonstrate their promise.

This review is organized as follows: the remainder of this section presents common broadband frequency conversion techniques (1.1) and outlines the historical progress of the adiabatic technique specifically (1.2). Section 2 reviews the theoretical foundations of adiabatic nonlinear frequency conversion under the undepleted pump approximation. Section 3 covers the theoretical and experimental extension to the fully nonlinear (depleted pump) regime in the quasi-monochromatic limit (i.e. with narrowband and chirped broadband pulses). Section 4 introduces a recent development—analysis and realization of all-ultrashort-pulse adiabatic frequency conversion with pump depletion. Section 5 discusses cascaded adiabatic processes and their applications. Section 6 presents adiabatic FWM. Section 7 discusses the significance of these advances within the context of ultrafast optics, in particular attosecond science, HHG and mid-IR spectroscopy. Section 8 concludes the article.

1.1. Summary of broadband frequency conversion techniques

Many techniques for broadband frequency conversion were suggested and demonstrated over the years (see figure 1). The earliest phase-matching method utilizes birefringence [18]. In this method, the refractive index's dependence on polarization compensates for its dependence on frequency. With the birefringence method, the conversion bandwidth can be increased by using a shorter nonlinear crystal. Unfortunately, shorter crystals provide lower conversion efficiency, resulting in a bandwidth-efficiency trade-off.

So-called random nonlinear materials (artificial or natural) lack long-range order while possessing a high degree of short-range order. This arrangement averages-out the effect of the phase-mismatch, since the generated wave's phase performs a random walk (rather than just 'walking off' the driving wave's phase). The

result is a large conversion bandwidth, determined by the material's short-range order statistics [22, 23]. However, this comes at the expense of efficiency: the phase's random walk degrades the coherent build-up of the generated wave along the medium.

Another common approach for phase-mismatch compensation is quasi-phase matching (QPM) via electric field poling [24]. In this technique, the sign of the crystal's nonlinear susceptibility is usually modulated (poled) in a periodic manner along the direction of propagation. The modulation period is chosen such that the phase of the generated wave is inverted where it is about to get out of phase with the propagating wave. QPM with periodic modulation suffers the same efficiency-bandwidth trade-off as birefringent phase-matching; however, some variations of this approach relax the trade-off to some degree: multi-periodic modulation [24], non-adiabatic chirp [25, 26] and adiabatic chirp [27, 28]. These techniques are rather complex but highly beneficial in terms of flexibility, robustness, bandwidth and efficiency.

With the multi-periodic design, the crystal is composed of multiple periodically-modulated sections. Each section quasi-phase matches a different, relatively narrow frequency range, and together they cover a broader range of frequencies than standard periodic designs. A significant disadvantage of this arrangement is that it produces a discontinuous conversion spectrum. If an ultrashort pulse with a broad and continuous spectrum is to be converted, its shape will not be preserved. Therefore, the multi-periodic design technique is suitable for multiple simultaneous narrowband processes but not for shape-preserving conversion of ultrashort pulses.

In chirped poling design the poling periodicity monotonically increases or decreases along the direction of propagation. The main advantage of the chirped design is its high bandwidth due to the wide range of compensated phase-mismatch values. However, a non-adiabatic chirped design introduces the usual trade-off between bandwidth and efficiency. In contrast, in an adiabatic chirp design, where the chirp rate is sufficiently low, high efficiency is maintained over a large bandwidth. Adiabatic frequency conversion is extremely useful, surpassing other methods in terms of efficiency, bandwidth and robustness. This technique is not limited to monotonically changing the periodicity of the poling—any pattern is possible as long as the rate of change is slow enough, i.e. the adiabaticity criterion is satisfied (detailed below). The conversion efficiency is uniform over a broad and continuous spectral range, offering pulse-shape-preserving conversion. This is extremely important for high-quality pulse shaping, generally a difficult task and not available at all frequencies with the same performance level. By using adiabatic conversion, the pulses can be shaped in a convenient spectral range and then converted to the desired range. Adiabatic conversion processes can also be cascaded to facilitate additional advantages (see section 5).

Though most widely used, chirped electric field poling QPM is not the only way to facilitate adiabatic frequency conversion. Additional approaches include temperature gradients [29, 30], electric field gradients [31], gas pressure gradients [32], and waveguide width variation [33, 34].

1.2. Adiabatic frequency conversion—timeline of progress

Over the past decade, adiabatic frequency conversion has gained popularity and was substantially expanded. In this section, we lay out an overview of this progress. Initial work focused on three-wave mixing (TWM) in the quasi-monochromatic undepleted pump regime. Interestingly, the quasi-monochromatic limit also applies when mixing a narrowband pump with broadband pulses, making it of interest to ultrafast applications as well. Under the undepleted pump approximation one of the interacting waves (usually termed 'pump') is much more intense than the other waves ('signal' and 'idler'), and therefore it is negligibly affected by the interaction. Later developments removed the undepleted pump requirement, increasing the efficiency and applicability of adiabatic frequency conversion to more types of sources and interactions, e.g. type I SHG. Recent advances broke out of the quasi-monochromatic regime, enabled all-short-pulse adiabatic frequency conversion and extended it to FWM processes. These recent approaches were experimentally demonstrated with ultrashort (few- and sub-cycle) and extremely wideband (more than octave-spanning) pulses in the fully nonlinear regime (depleted pump). Figure 2 presents the different regimes of adiabatic frequency conversion.

The first published experimental realization of adiabatic frequency conversion was made by Suchowski *et al* [27], who utilized an adiabatically chirped-poled crystal. They demonstrated sum-frequency generation (SFG) conversion of a tunable 5 ns pulse over a 140 nm (∼17.7 THz) bandwidth from the near-IR (1470–1610 nm) to the visible range with more than 50% efficiency over the FWHM range, reaching peak efficiency of 74%. Prior to this achievement, standard periodic poling technique was able to achieve bandwidth on the order of only 2 nm. At this point and over the next few years, theoretical modeling and experiments remained in the undepleted pump regime. These showed the conversion efficiency to be insensitive to input wavelength, crystal temperature and length, pump intensity and angle of incidence [35]. For example, high efficiency over a large conversion bandwidth was shown to be conserved over temperature variation of more than 100 °C.

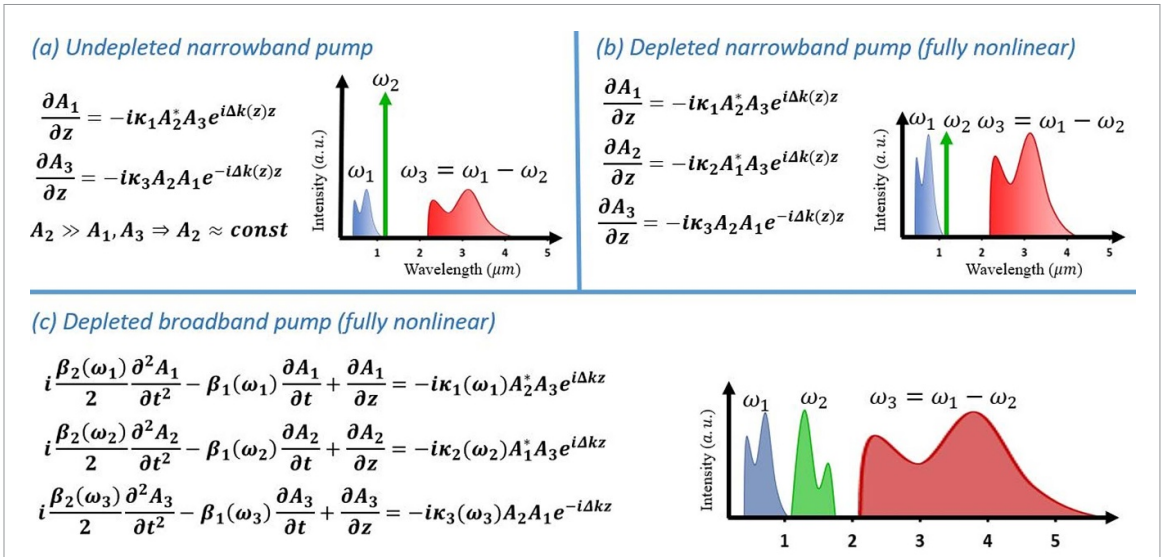

Figure 2. Regimes of adiabatic frequency conversion. (a) Undepleted narrowband pump. The color gradient represents chirp. (b) Depleted narrowband pump (fully nonlinear). (c) Depleted broadband pump (fully nonlinear).

Over 2011–2014, several experiments demonstrated how adiabatic frequency conversion under the quasi-monochromatic approximation is indeed useful for ultrafast optics applications, even at the extreme of octave-spanning bandwidth [36–39]. In all of these cases, near-IR stretched or uncompressed broadband sources of picosecond duration were upconverted into the visible range or downconverted into the mid-IR range. Importantly, the broad conversion bandwidth implied pulse-shape preservation. Significant milestones include the generation of an octave in the mid-IR, spanning 2–5 μm, with near-100% conversion efficiency [38], and the generation of visible light spanning 405–500 nm with 92% conversion efficiency [39].

After achieving these benchmarks, the established adiabatic technique was used to facilitate temporal-shaping of mid-IR pulses. Krogen *et al* [19] shaped and stretched near-IR pulses, converted them to the mid-IR, and then compressed them, showing that the conversion process preserved the pulse shape. They were able to demonstrate generation and multi-octave shaping of high-energy (μJ scale) mid-infrared single-cycle pulses (11 fs, 1.2 optical cycles) with a spectral span of 1.8–4.4 μm.

Simultaneously, progress has been made with adiabatic optical parametric amplification (OPA) [40–46] for high repetition rate ultrashort (few-cycle) mid-IR pulse generation from available near-IR sources, such as Ti:Sapphire. This was done with a view towards HHG research. A recent experiment exhibited the generation of 14.4 fs pulses centered at 2.5 μm at a repetition rate of 100 kHz with average power of 12.6 W, achieving high peak power of 6.3 GW [47].

Significant advancements were made by expanding adiabatic frequency conversion to the fully nonlinear regime, i.e. removing the undepleted pump approximation, but remaining in the quasi-monochromatic regime [41, 48, 49]. The first demonstration of adiabatic SHG achieved 86% conversion efficiency of a stretched femtosecond pulse in a $LiNbO_3$ waveguide [50]. In a bulk KTP crystal, adiabatic SHG of nanosecond pulses achieved 73% efficiency with temperature acceptance bandwidth of >100 °C [51]. Both used adiabatically chirped poling designs.

Next, the adiabatic approach was expanded to include the short-pulse regime outside the quasi-monochromatic approximation. The first experimental demonstration achieved SHG of ultrafast (300 fs) pulses with 30% efficiency, limited by parasitic nonlinearities [52]. Later experimental work frequency-doubled short and shaped pulses. The SHG was pulse shaped while achieving 50% conversion efficiency [20]. Notably, high-efficiency SHG of ultrashort (sub-picosecond) pulses had been realized earlier [53] but over a bandwidth of 8 nm, significantly smaller than the 75 nm bandwidth that was achieved with the adiabatic design.

Adiabatic frequency conversion has been realized by additional approaches besides the chirped poling technique. Markov *et al* [29] facilitated adiabatic OPA of a 700 fs source by applying a controlled temperature gradient to a 5 cm long LBO crystal. The experiment demonstrated 45% conversion efficiency over a bandwidth of 300 nm in the near-IR. Rozenberg *et al* [30] used the same technique with a large-aperture (5 × 5 mm) LBO crystal. This showed that adiabatic temperature gradients could facilitate higher power scaling (while avoiding laser induced damage) as compared to poling (which is limited to ∼1 mm apertures). Liu *et al* [31] presented a third approach. They applied an electric-field gradient along a crystal, which

resulted in adiabatic phase-mismatch variation through the electro-optic effect. The temperature- and electric-field-gradient techniques make it possible to implement adiabatic frequency conversion with additional materials, i.e. not only those that are amenable to poling. These materials have advantageous properties, such as high damage thresholds, transparency in the UV and/or mid-IR, large apertures and high thermal conductivity (enabling power scaling). Additionally, as opposed to poling, these methods provide *in situ* configurability and fine-tuning.

Very recently, the adiabatic technique was theoretically extended to include FWM in $\chi^{(3)}$ nonlinear platforms, such as silicon photonics and optical fibers [54]. Highly efficient (90%) conversion of a 1.62–1.72 μm source to 1.78–1.86 μm is predicted in an adiabatically-tapered silicon waveguide. Initial experiments in a linearly-tapered highly-nonlinear photonic crystal fiber (PCF) show 60%–70% conversion efficiency of nanojoule pulses from a near-IR band (696–723 nm) to the mid-IR (2.15–2.43 μm) [33]. A recent numerical analysis considers broadband generation of mid-IR light via adiabatic FWM in a linearly-tapered anti-resonant hollow-core fiber (AR HCF) with a simultaneous pressure gradient [32]. This work predicts 70% conversion efficiency of a 26 fs pulse from near-IR to mid-IR, generating a 3–5 μm spectrum. The linear transfer function survives to idler pulse energies above 10 μJ, making the technique relevant to strong-field science. A similar approach in large-core hollow capillary fibers may allow scaling to much higher energies. As adiabatic FWM is a very recent development, more exciting implementations and advances are expected in the near future.

In the following sections, we introduce the theoretical foundation of adiabatic frequency conversion. The summarized theoretical analysis is interlaced with examples of significant landmarks and contemporary applications.

2. Adiabatic frequency conversion in the undepleted pump regime: from quasi-monochromatic to ultrafast

In this section we present the fundamentals of adiabatic frequency conversion as a basis to exploring the dynamics of this interaction. Further information and in-depth analysis can be found in other sources [18, 28]. We begin by describing the dynamics in a relatively simple case, i.e. in the quasi-monochromatic regime under the undepleted pump approximation. We use the term quasi-monochromatic to refer to the case where the pump field (ω_2) is significantly narrowband to approximate a one-to-one conversion between the other frequencies: $\omega_3\,(\omega_1) \approx \omega_1 - \omega_2$, where ω_2 is constant. Throughout the next sections we gradually relax these approximations, advancing towards more general cases. The most general case involves interactions where all pulses are ultrashort ($\ll$1 picosecond), in the fully-nonlinear (depleted pump) regime.

2.1. Nonlinear susceptibility

Nonlinear optical phenomena occur when the optical properties of matter are modified by the presence of light. The modification depends nonlinearly on the amplitude of the applied field. New frequencies can be generated as a consequence of the nonlinear light–matter interaction. In most cases, the optical field can be treated as a perturbation to the internal field in the medium. The induced polarization in these cases can be expressed as:

$$\vec{P} = \vec{P}_{\text{Linear}} + \vec{P}_{\text{Nonlinear}} = \underbrace{\varepsilon_0\chi^{(1)}\vec{E}}_{\vec{P}_{\text{Linear}}} + \underbrace{\varepsilon_0\chi^{(2)}\vec{E}^2 + \varepsilon_0\chi^{(3)}\vec{E}^3 + \cdots}_{\vec{P}_{\text{Nonlinear}}} \tag{1}$$

where $\chi^{(2)}, \chi^{(3)}$ are the second- and third-order nonlinear susceptibilities, respectively, unique properties of each dielectric material [18]. Notably, only non-centrosymmetric materials have nonzero even-order nonlinear susceptibilities, such as $\chi^{(2)}$. Most commonly, the lowest-order nonlinear susceptibility dominates the nonlinear optical response. The presence of a field, possibly containing multiple frequencies (e.g. ω_1 and ω_2), results in the generation of new frequencies that were not incident onto the material. A few examples of such TWM processes, a result of non-zero second-order susceptibility, are $\omega_3 = \omega_1 + \omega_1 = 2\omega_1$ (SHG), $\omega_3 = \omega_1 + \omega_2$ (SFG) and $\omega_3 = |\omega_1 - \omega_2|$ (difference frequency generation, DFG). Similarly, there are FWM processes due to the third-order susceptibility.

2.2. Nonlinear coupled wave equations and QPM

In the case of TWM, where the nonlinear polarization is limited to the second-order nonlinear term, the interaction is governed by three coupled nonlinear wave equations:

$$\frac{\mathrm{d}A_1(z)}{\mathrm{d}z} = i\kappa_1 A_2^* A_3 \mathrm{e}^{-i\Delta k z}$$

$$\frac{\mathrm{d}A_2(z)}{\mathrm{d}z} = i\kappa_2 A_1^* A_3 \mathrm{e}^{-i\Delta k z}$$

$$\frac{\mathrm{d}A_3(z)}{\mathrm{d}z} = i\kappa_3 A_1 A_2 \mathrm{e}^{+i\Delta k z}, \tag{2}$$

where A_j are the amplitudes of the electric fields ($j = 1, 2, 3$ are usually termed 'signal', 'pump' and 'idler', respectively), $\kappa_j = \frac{\omega_j \chi^{(2)}}{cn(\omega_j)}$ are the coupling coefficient, $k_j = \frac{n(\omega_j)\cdot\omega_j}{c}$ are the wavenumbers and $n(\omega_j)$ are the frequency-dependent refractive indices of the material. The term $\Delta k = k_1 + k_2 - k_3$ is the phase mismatch. The phase mismatch can significantly affect the efficiency of the conversion process. Equation (2) describe monochromatic waves, where the index of refraction can be regarded as a constant for each wave. For modeling short pulses, the index must be explicitly calculated for each frequency within the bandwidth of each wave. The nonlinear susceptibility $\chi^{(2)}$ is generally frequency dependent as well, but usually this dependence is very weak and can be neglected [18]. In the remainder of this section we will elaborate on the importance of the phase mismatch and present common phase-matching techniques. Later these will be used to facilitate adiabatic evolution.

The phase mismatch arises due to the dispersive nature of matter: the refractive index depends on frequency, and therefore each of the interacting waves propagates through the medium at a different phase velocity. The incident and generated waves are coupled through the nonlinear polarization. Depending on the relative phase between the waves, energy will flow either from the incident waves to the generated wave, or vice versa. Since these waves have different phase-velocities, their relative phases change as they propagate through the medium. Consequently, the direction of energy flow alternates along the medium, resulting in a low net flow, i.e. low conversion efficiency.

The coherence length parameter, defined $l_c \equiv \pi/\Delta k$, is a measure of the spatial distance that is sufficient to cause the waves to get out of phase with each other. When that happens, the direction of energy flow is reversed, a phenomenon called back-conversion. For example, in DFG, instead of energy flowing from the pump and signal to the idler, energy will flow from the idler to the pump and signal. This reversal repeats every l_c propagation distance (commonly $\sim$10 μm), effectively preventing the build-up of the desired idler wave and lowering the efficiency of the process. Naively, one can design the crystal to the exact length that is required for the maximum build-up of the interaction, but the limited interaction length (order of 10 μm) will result in very low conversion efficiency.

2.3. Adiabatic frequency conversion and adiabaticity criterion

One of the main drawbacks of the periodic QPM design is that it is relatively narrowband, i.e. the range of frequencies for which phase matching can be achieved with this technique is relatively small. Modulating the susceptibility in an aperiodic manner, e.g. by varying the lengths of the modulation sections along the direction of propagation, can increase the range of frequencies for which phase matching can be achieved. This was demonstrated with (non-adiabatic) chirped QPM designs, where significantly larger bandwidth was achieved at the expense of efficiency. If the rate of change of the modulation period is small enough, the interaction becomes adiabatic.

In adiabatic evolution a system remains in one of its eigenstates throughout the interaction, while the character of the eigenstate gradually transforms. This can occur when system variables vary at a much slower rate than the internal dynamics of the system. This allows the dynamical system to adapt to the changes and remain in an eigenstate. The adiabaticity criterion is [28]

$$\left|\frac{d\Delta k}{\mathrm{d}z}\right| \ll \frac{\left(\kappa^2 + \Delta k^2\right)^{\frac{3}{2}}}{|\kappa|}. \tag{3}$$

We note that, in the undepleted pump approximation, the dynamics of TWM possess SU(2) symmetry. This makes it analogous with linear two-level systems, such as the interaction of coherent light with a two-level atom, spin 1/2 dynamics in NMR, etc [28].

An adiabatic process transfers all of the energy from the eigenstate's initial form to its final form. For example, the initial and final forms of the eigenstate could correspond to different distributions of energy between optical frequencies. As theoretical and experimental results that are presented in this review show, this technique eliminates the efficiency-bandwidth trade-off.

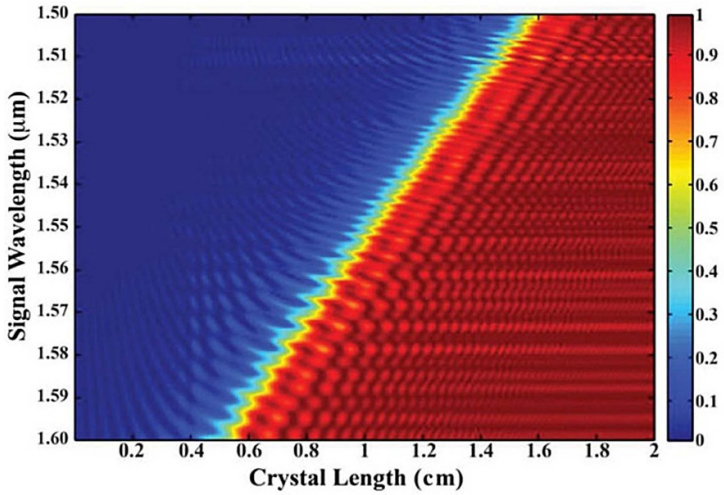

Figure 3. Adiabatic conversion scheme. Conversion efficiency for the adiabatic chirp design along the propagation axis (horizontal axis) and different input wavelength (vertical axis). Reprinted from [28] with permission from John Wiley & Sons. © 2013 by WILEY-VCH Verlag GmbH & Co. KGaA, Weinheim.

The adiabaticity criterion requires that the phase mismatch parameter, $\Delta k(z)$, should be very large compared to the coupling coefficient in the edges of the crystal, i.e. $|\Delta k|_{z=0,L_c} \gg \kappa$, slowly varying from large negative (positive) to large positive (negative) value (i.e. $\Delta k < 0$ at the beginning of the crystal and $\Delta k > 0$ at the end or vice versa). The exact manner of variation throughout the crystal is of secondary importance as long as it meets the adiabaticity criterion.

2.4. Adiabatic frequency conversion of broadband sources

The theoretical analysis presented so far in the context of monochromatic waves is also valid in the case of broadband sources, as long as each spectral component can be treated separately as a quasi-monochromatic source. This requirement can be fulfilled by stretching short pulses, e.g. from femtosecond transform-limited duration to durations on the order of few picoseconds, and employing a relatively narrowband pump pulse, such that a one-to-one conversion relationship is established between the frequencies of the other waves, $\omega_3(\omega_1) \approx \omega_1 - \omega_2$, where ω_2 is constant.

In this case, the phase-matching condition $\Delta k \approx 0$ is satisfied over a very short distance for each wavelength, and occurs at different longitudinal positions in the nonlinear medium. The effective interaction length, over which a significant exchange of energy between waves at different frequencies occur, is smaller than crystal length (usually on the order of 10 mm). One may think of a broadband frequency conversion device in this regime as consisting of a continuous superposition of monochromatic adiabatic conversion devices. The fact that the effective interaction length is shorter than the device length also helps to partially mitigate the impact of GVM, as discussed below.

Figure 3 shows a simulation of adiabatic evolution of a frequency conversion process with more than 12 THz bandwidth reaching nearly 100% efficiency in a single 20 mm long chirped crystal, using equation (2) to model each signal frequency component in the pulse. The adiabatically varying phase-mismatch offers a significant improvement over the periodic design by eliminating back conversion, due to the fact that each frequency has a short range in which it is phase-matched—the idler does not have the opportunity to be converted back to the signal. Each signal frequency is seen to convert efficiently to its corresponding idler at a different longitudinal coordinate.

The Landau–Zener theorem [55, 56] provides the analytical asymptotic solution for ideal adiabatic evolution of a linear SU(2) system. It was adapted to frequency conversion [28] and can be used as an asymptotic approximation of conversion efficiency:

$$\eta_{\mathrm{LZ}}(z \to \infty) = 1 - \mathrm{e}^{-\frac{2\pi|\kappa|^2}{|d\Delta k/\mathrm{d}z|}}. \tag{4}$$

The expression is precise when the phase mismatch varies linearly and is an approximation otherwise. Adiabatic evolution occurs when the adiabatic parameter $\alpha \equiv \frac{|d\Delta k/\mathrm{d}z|}{2\pi|\kappa|^2}$ is very small (i.e. $\alpha \ll 1$). This limit is approached as the phase mismatch variation rate decreases and as the coupling coefficient increases (e.g. due to increased pump intensity). This theoretical analysis was experimentally validated for ultrashort pulses by Moses *et al* [37]. They converted 0.7-octave spanning Ti:Sapphire pulses from near-IR to mid-IR in a DFG

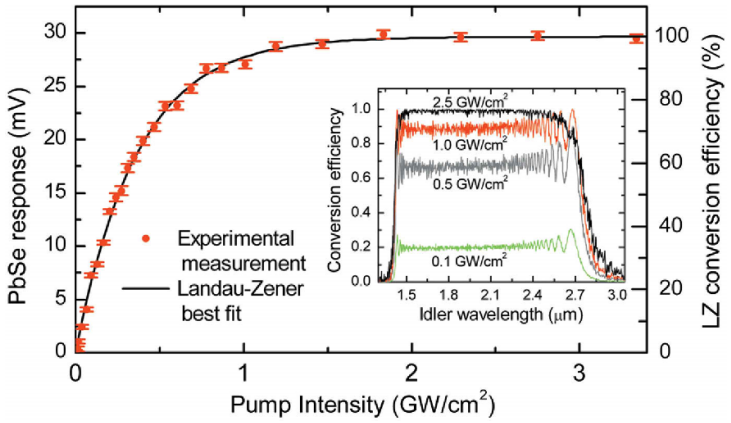

Figure 4. Measured PbSe photodiode response plotted versus peak pump intensity. Error bars indicate the relative measurement error. Solid line: exponential fit $A\,(1-\exp[BI_2])$ of the experimental data. The adjusted $R^2 = 0.998$. Inset: predicted conversion efficiency versus idler wavelength for several pump intensities based on numerical simulations. Reproduced with permission from [37].

process, reaching near-100% efficiency, using an adiabatic chirp-poled potassium titanyl phosphate crystal. The main result is shown in figure 4.

When mixing broadband pulses, the high-order dispersive properties of the nonlinear medium must be taken into consideration. The refractive index significantly varies within the bandwidth of the waves and it is no longer sufficient to consider it constant according to the center wavelength of each wave. Two significant phenomena that arise from this variation and substantially affect the propagation and interaction of the waves are GVM and GVD.

GVM, the first order dispersion term, causes longitudinal walk-off between pulses with different carrier frequencies due to their distinct group velocities. It is characterized by the distance over which pulses with different carrier frequencies sufficiently overlap, termed quasi-static interaction length: $L_{\mathrm{QS}} = \tau/\mathrm{GVM}$, where τ is the FWHM pulse duration and GVM is the difference between the inverse group velocities of the pulses, $\mathrm{GVM} = \left|\frac{1}{v_{\mathrm{g1}}} - \frac{1}{v_{\mathrm{g2}}}\right|$. To overcome the GVM limitation in short-pulse frequency conversion, the quasi-static interaction length should be significantly larger than the typical adiabatic conversion length: $L_{\mathrm{QS}} \gg L_{\mathrm{adiabatic}} = \frac{\kappa}{|d\Delta k/\mathrm{d}z|}$ [28]. Combining the last equations, we obtain a fundamental limit for the minimum acceptable pulse duration. For example, in the case of SFG of a broadband signal with a narrowband pump, the minimum acceptable pulse duration is

$$\tau_{\min} \geqslant L_{\mathrm{adiabatic}} \cdot \mathrm{GVM} = \left|\frac{\kappa}{d\Delta k/\mathrm{d}z}\left(\frac{1}{v_{\mathrm{g,s}}} - \frac{1}{v_{\mathrm{g,i}}}\right)\right|, \tag{5}$$

where $v_{\mathrm{g,s}}$ and $v_{\mathrm{g,i}}$ are the group velocities of the signal and idler, respectively. Typically, pulse duration on the order of a few picoseconds is sufficient for efficient broadband conversion in the visible and near infrared spectral ranges.

GVD, the second order dispersion term, leads to temporal spreading of the broadband pulses. In the case of ultrafast signal and idler pulses with a narrowband undepleted pump, several possible issues must be considered. If the signal and idler pulses spread enough to grow longer in duration than the pump, part of their chirped spectra may no longer overlap with the pump pulse, eliminating the nonlinear interaction. Alternatively, opposite GVD may dechirp the signal or idler, increasing these waves intensity. In that case, their intensities may approach or even exceed the intensity of the pump, thus violating the undepleted pump approximation.

GVD is defined as $\beta = \frac{\mathrm{d}^2\omega}{\mathrm{d}k^2}$ and has a characteristic length of $L_{\mathrm{GVD}} = \frac{\tau^2}{\beta}$. For the case of a highly chirped signal pulse, the adiabatic length may cover several GVD lengths without a significant change in the signal pulse duration. This fact is used to the advantage of the pulse shaping scheme outlined in section 2.5. However, in the case of unchirped pulses and also the case where the pump pulse is broadband (see section 4), in order to achieve efficient conversion, it is generally required that the GVD length is significantly longer than the adiabatic interaction length. The implication of this demand is that the conversion occurs over a distance in which the GVD is negligibly small. This can be achieved by making sure $L_{\mathrm{GVD}} \gg L_{\mathrm{adiabatic}}$ for the shortest GVD characteristic length, typically corresponding to the shortest wavelength.

2.5. Linearity of spectral transfer function and ultrafast pulse shaping

For the case of a relatively narrowband pump pulse and undepleted pump, the one-to-one photon transfer between signal and idler implies a linear transfer function in spectral amplitude, where the ratio of idler to signal intensity is $I_i = (\omega_i/\omega_s) I_s$. The linear spectral amplitude transfer function for ultrafast pulses was observed in Moses *et al* [37] as well as in a greater than octave-spanning adiabatic downconversion experiment in which a chirped 680–870 nm signal pulse was mixed with a relatively narrowband 1047 nm 12 ps pulse in an adiabatically chirped lithium niobate crystal to generate an idler spectrum covering 2–5 μm [38].

In their follow-on experiment [19], the same researchers observed the expected linear spectral *phase* transfer function spanning the entire generated 1.8–4.4 μm idler spectrum. Confirmed by the experiment as well as by a numerical solution of the pulse propagation equations (including exact dispersion across the full spectral extent of signal, pump, and idler waves), the authors found that the total group delay dispersion (GDD) of the device was well approximated by

$$\tau(\omega_i) = k'(\omega_s) z_c(\omega_s) + k'(\omega_i)(L - z_c(\omega_s)), \tag{6}$$

where $k(\omega_s)$ and $k(\omega_i)$ are the signal and idler wavenumbers, $k'(\omega)$ is $\partial k(\omega)/\partial\omega$, $z_c(\omega_s)$ is the frequency dependent conversion position (i.e. where $\Delta k(\omega_s) = 0$), and L is the length of the crystal. In other words, for each converted photon, to determine the total group delay accumulated in the device, the device can be broken into two sections, a first section where group delay is accumulated at the group velocity of the signal frequency prior to conversion, and a second section where the group delay is accumulated at the group velocity of the idler following conversion.

The linearity of both phase and amplitude spectral transfer functions was utilized in Krogen *et al* [19] for the shaping of the generated octave-spanning idler pulses. Figure 5 illustrates the scheme. The chirped (uncompressed) signal from a 10 fs near-IR OPCPA system was combined with 12 ps pulses from the OPCPA pump laser in the adiabatically poled lithium niobate crystal, generating the chirped 1.8–4.4 μm idler spectrum, with a relative spectral phase given by the linear transfer function, equation (6). By modifying the phase function sent to a programmable pulse shaper located in the OPCPA, an additional pre-chirp was added to the already chirped signal pulse, tailored to eliminate residual high-order dispersion on the DFG idler pulse after a bulk silicon compressor. This led to the generation of 11 fs pulses—1.1× the transform-limited duration—corresponding to 1.2 optical cycles of the 2.8 μm central wavelength of the idler (see figure 5(b)).

The scheme made use of several features of adiabatic frequency conversion in the undepleted pump regime with a relatively narrowband pump (quasi-monocromatic approximation): since significant changes to the spectral amplitude and phase profiles of the signal can be made without affecting the efficiency of the downconversion process, the spectral amplitude and phase profiles of the octave-spanning idler pulse can be tuned directly by means of the near-IR pulse shaper. Precisely, as photon conversion from signal to idler is one-to-one, any amplitude shaping imparted on the near-IR signal is directly transferred to the idler. As for the phase, any differential phase added to the signal by means of the pulse shaper will appear as the identical differential phase added to the idler, without any additional changes to its power spectrum. For example, by applying an additional ⟦sin⟧^2 spectral amplitude function and sawtooth phase function to the signal pulse shown in figure 5(b), the idler pulse was split into the corresponding mid-IR single-cycle pulse pair with arbitrary inter-pulse delay (figure 5(c)). Third, since the downconversion process increases the relative bandwidth of the pulse (absolute bandwidth is maintained while central frequency is decreased), an ordinary few-cycle pulse shaper in the near-IR was used to shape the bandwidth of the generated 1.3-octave mid-IR pulse. The arbitrary pulse shaping of greater than octave-spanning pulses is thus a special characteristic of adiabatic frequency conversion in this regime, and it may benefit strong-field physics applications as well as ultrafast time-resolved spectroscopy.

Finally, Flemens *et al* noted that there is substantial room to vary the function $z_c(\omega_s)$ in equation (6) through the design of the frequency conversion device's poling function without spoiling the adiabatic conversion. Thus, the GDD of the device can be modified, and such 'intrinsic' pulse shaping might be used to simplify the dispersion management of an octave-spanning device [57]. The authors numerically simulated a poled lithium niobate device for generating a 2.0–4.0 μm idler that has a total GDD of nearly zero. The study predicted that an 8 fs (unchirped) near-IR pulse can be converted to an unchirped 9 fs mid-IR pulse at the output of the device. The device is designed to allow the normal GVD of the material for the signal wavelengths to chirp the signal to picosecond duration before adiabatic conversion occurs, and then exactly de-chirp the idler pulse through the anomalous GVD of the idler wavelengths after conversion, producing a recompressed idler at the device's exit.

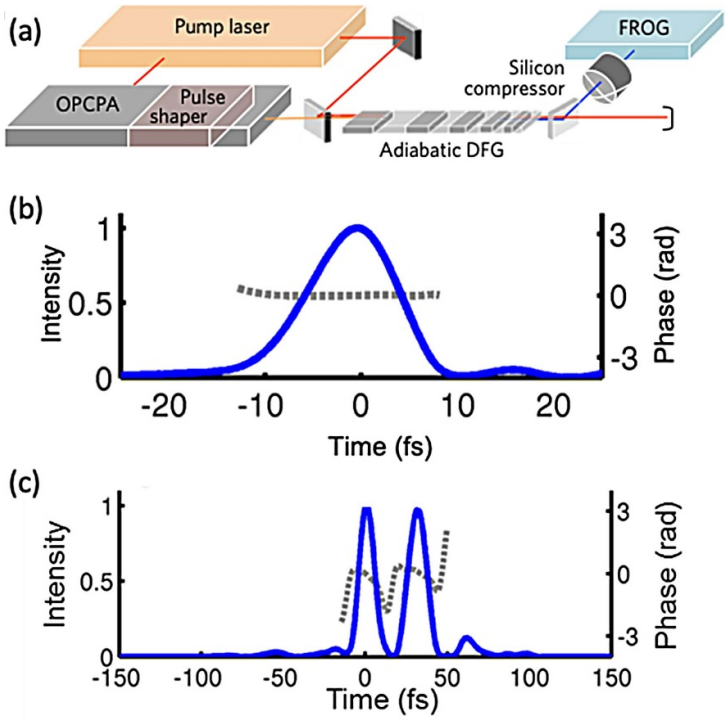

Figure 5. (a) Scheme for the generating and arbitrary shaping of octave-spanning mid-IR pulses. An adiabatic DFG stage is inserted prior to the compressor of an OPCPA system to convert a chirped 10 fs near-IR pulse to a chirped 11 fs mid-IR pulse. A programmable pulse shaper in the OPCPA before the adiabatic frequency conversion stage pre-compensates for the residual dispersion in the system to high orders, producing a near-transform-limited single-cycle mid-IR pulse after the compressor. (b) By further tuning the shaping function, this single-cycle pulse could be manipulated to generate a complex pulse shape. A single-cycle pulse pair was demonstrated. (c) Adapted and reprinted from [19] with permission of Springer Nature, © 2017.

3. Adiabatic frequency conversion with pump depletion (fully-nonlinear regime)

Frequency conversion in the fully nonlinear regime is a generalization of the dynamics that were discussed earlier. In the fully nonlinear regime, it is no longer assumed that one of the waves is significantly more intense than the others and negligibly affected by the interaction. The coupled equations can no longer be linearized and the analogy to linear SU(2) systems does not hold. The dynamics in the fully nonlinear regime are more complex, leading to some difficulties in reaching high efficiency and robustness. However, for monochromatic waves, the dynamics can be cast into a canonical Hamiltonian form, and the classical mechanics adiabatic invariance theorem [58] can be used. This theorem applies to any canonical Hamiltonian system, linear or nonlinear. In this section we consider narrowband and chirped broadband pulses, cases in which the analytical framework for monochromatic waves can be used to make accurate predictions of the dynamics. The next section extends these concepts to the ultrashort compressed pulse regime.

We describe the dynamics of the system in a canonical Hamiltonian structure. The Hamiltonian depends on a single system parameter, the phase mismatch. According to the classical adiabatic invariance theorem, if the phase mismatch varies much more slowly than the system's internal dynamical rate of variation, then the system state will follow an eigenstate. The coupled wave equation (2) can be reformulated in the canonical Hamiltonian structure

$$\frac{\mathrm{d}Q_1}{\mathrm{d}\xi} = \frac{\partial H}{\partial P_1}$$
$$\frac{\mathrm{d}P_1}{\mathrm{d}\xi} = \frac{\partial H}{\partial Q_1}, \tag{7}$$

where the canonical momentum P_1 is the excess of photon flux of the two incident waves over the generated wave, the canonical coordinate Q_1 is proportional to the phase difference between the incident waves and generated wave, $\xi = z/\sqrt{\kappa_1\kappa_2\kappa_3}$ is a scaled propagation length and H is the Hamiltonian. The exact mathematical expressions of these quantities are given elsewhere [49]. Here we note that the Hamiltonian depends only on constants of the motion (Manley–Rowe constants), the phase-mismatch, and the dynamical variables P_1 and Q_1.

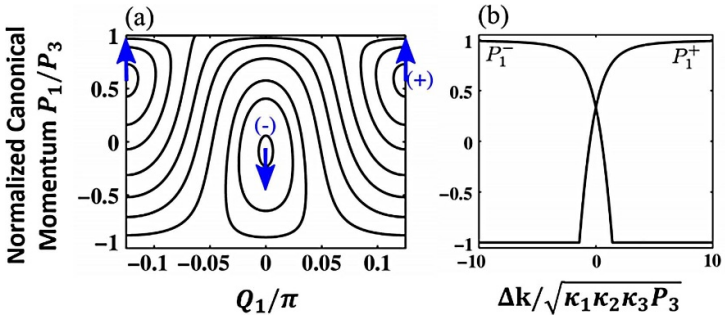

Figure 6. (a) Exemplary phase space portrait of the canonical Hamiltonian representation of TWM. Arrows indicate motion of fixed points (corresponding to eigenstates) with increasing phase-mismatch. (b) Normalized canonical momentum for the two eigenstates versus $\Delta k/\sqrt{\kappa_1\kappa_2\kappa_3 P_3}$, a normalized phase-mismatch parameter. Reproduced with permission from [49].

Figure 6(a) displays an exemplary phase space portrait. The phase mismatch is non-zero. The fixed points (marked with + or −) correspond to eigenstates; the arrows indicate the direction of motion of the fixed points with increasing phase mismatch.

Figure 6(b) displays the corresponding canonical momentum $P_1^{\pm}$ (vertical position in the phase space) of the two eigenstates, normalized to the total photon flux P_3, versus the normalized phase mismatch $\Delta k/\sqrt{\kappa_1\kappa_2\kappa_3 P_3}$. P_1^- is seen to be a monotonically decreasing function of the phase mismatch, beginning at $P_1^- \approx P_3$ for a very large negative phase-mismatch and reaching $P_1^- \approx -P_3$ for a large positive phase-mismatch. In the same figure (and in general), P_1^+ has the opposite behavior to P_1^-, i.e. $P_1^+(\Delta k) = P_1^-(-\Delta k)$. Physically, this means that the eigenstate labeled with a minus corresponds to having all of the energy in the incident waves when the phase-mismatch is large and negative. When the phase-mismatch is large and positive, this eigenstate corresponds to having all of the energy in the generated wave. For the plus eigenstate, the opposite is true.

If the phase-mismatch varies adiabatically from a large negative value to a large positive value (or vice-versa), the system will evolve adiabatically. Then the system state can follow one of the two eigenstates as the eigenstate changes its character in accordance with the variation in the phase-mismatch. This change corresponds to fully efficient frequency conversion. Porat *et al* [49] provided an analytical solution for the case of an adiabatic process where the two low frequencies have equal photon flux.

For adiabatic evolution to occur, the system has to be initially close to an eigenstate (easily satisfied by a large initial phase-mismatch), and the rate of change of the phase mismatch has to be small enough to satisfy [49]

$$r_{\mathrm{nl}} = \left| \sqrt{\kappa_1\kappa_2\kappa_3}\frac{\mathrm{d}\left(P_1^{\pm}/P_3\right)}{d\Delta\mathrm{k}}\frac{d\Delta\mathrm{k}}{\mathrm{d}z} \right| \nu^{-1} \ll 1, \tag{8}$$

where ν is the frequency at which the system point orbits a fixed point.

This technique is broadband and robust because the phase mismatch is swept over a large span. Changes in temperature and wavelength, which other methods are relatively sensitive to, have a much smaller impact in the adiabatic case. The FWHM phase-matching bandwidth of the process is approximately [49]

$$\Delta k_{\mathrm{BW}} = \Delta k|_{\mathrm{end}} - \Delta k|_{\mathrm{start}}. \tag{9}$$

Notably, it depends only on the chirp range of the phase-mismatch. An example of a numerical simulation of adiabatic SHG from Porat *et al* [49] is presented in figure 7.

The QPM period in a 40 mm long MgO-doped $LiNbO_3$ crystal with $\chi^{(2)} = 50$ pm V^{-1} was linearly chirped from 18.83 μm to 19.44 μm (corresponding to $\Delta k/\sqrt{\kappa_1\kappa_2\kappa_3 P_3}$ variation from −3 to +3 for input intensity of 200 MW cm^{-2} with $\lambda_1 = 1.55$ μm). The simulated conversion efficiency was 96% over a bandwidth of 42 nm.

Leshem *et al* used adiabatic SHG to experimentally explore the transition from the undepleted pump to the fully nonlinear regime, with nanosecond pulses [51]. In essence, their findings confirmed the theoretical analysis summarized above. Furthermore, they were able to demonstrate ∼60% and ∼80% conversion efficiency over temperature ranges of > 100 °C and 30 °C, correspondingly. This experiment used chirp-poled KTP crystals.

The first demonstration of ultrafast adiabatic SHG [50, 59] used strongly-chirped pulses, in the limit where the quasi-monochromatic approximation holds. In this experiment, a stretched pulse having 2.5 nJ

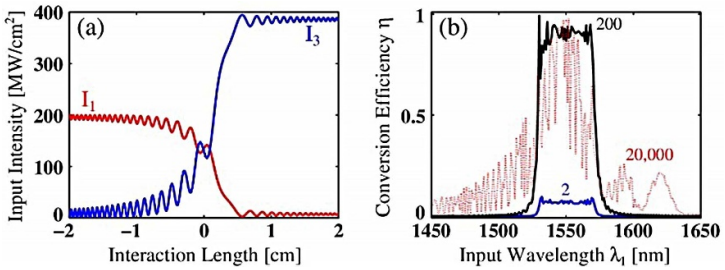

Figure 7. Adiabatic SHG with pump depletion. (a) Intensities along the crystal for input wavelength $\lambda_1 = 1550$ nm and input intensity 200 MW cm^{-2}. (b) Conversion efficiency versus input wavelength λ_1 for different input intensities, which are indicated in units of MW cm^{-2}. Only the 200 MW cm^{-2} case satisfies the adiabatic evolution requirements. Reproduced with permission from [49].

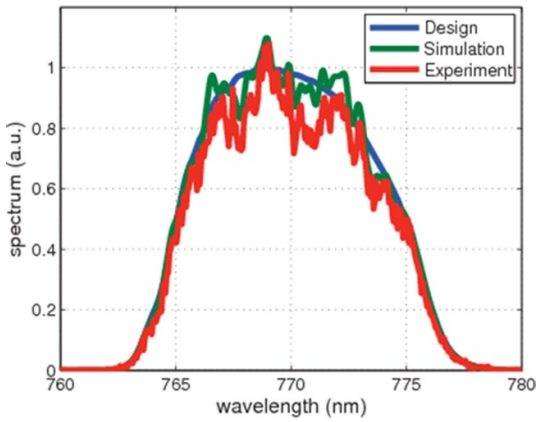

Figure 8. SH spectrum of a chirped 150 fs 1.5 μm pump in a chirped QPM $LiNbO_3$ waveguide. The blue line is the theoretical result for the nominal design, the green line is the simulation result using the actual imperfect waveguide and the red line is the experimental result. Reproduced with permission from [50].

energy, 1.55 μm central wavelength and 150 fs transform-limited duration was frequency-doubled in a $LiNbO_3$ waveguide. The crystal was chirp-poled to facilitate adiabatic SHG, achieving 86% conversion efficiency. Figure 8 shows excellent agreement between calculated and measured spectra.

In the context of broadband mid-IR source generation, extensive work has been carried out with OPAs. An early demonstration of pulse conversion and amplification utilizing the chirped-poling technique was carried out by Heese *et al* [42]. Later work by the same group [45, 46] demonstrated few-cycle pulses in different mid-IR regions, achieving higher intensities and shorter pulses at higher repetition rates. In these works, the signals were shaped and stretched before amplification, then amplified in multiple stages and eventually compressed to ultrashort durations. The first stages were high-gain pre-amplifiers where the pump was significantly stronger than the seed signal and generated idler. The last amplification stages were saturated power amplifiers with significant pump depletion. In Mayer *et al* [46], after compression, pulse duration of 44.2 fs and a pulse energy of 21.8 μJ at a repetition rate of 50 kHz were obtained, utilizing a non-collinear power amplifier stage.

Fully-nonlinear adiabatic frequency conversion has also been experimentally demonstrated by applying the temperature gradient technique. Markov *et al* [29] achieved over 50% conversion efficiency over a tuning range of more than 200 nm in the near-IR. They used adiabatic temperature-gradients across a bulk LBO crystal. A schematic setup and the main result are shown in figure 9 below. The converted source in this experiment was a 700 fs laser, yet is was very well modeled in the quasi-monochromatic approximation.

In another experimental demonstration, the temperature gradient approach was shown to facilitate power-scaling. The most commonly used method for implementing QPM is electric field poling. This method places restrictions on crystal aperture. Usually the crystal has to be no more than 1 mm thick in one transverse direction. This implies a maximum incident beam size, which in turn limits the maximum incident power that avoids damaging the crystal. Rozenberg *et al* [30] demonstrated adiabatic SHG with a large-aperture (5 $\times$ 5 mm) LBO crystal that was subjected to an adiabatic temperature gradient.

They achieved 60% conversion efficiency of a near-IR nanosecond laser. Compared to using a uniform temperature, the conversion efficiency was about twice as high and the temperature bandwidth was 5.4 times larger (see figure 10).

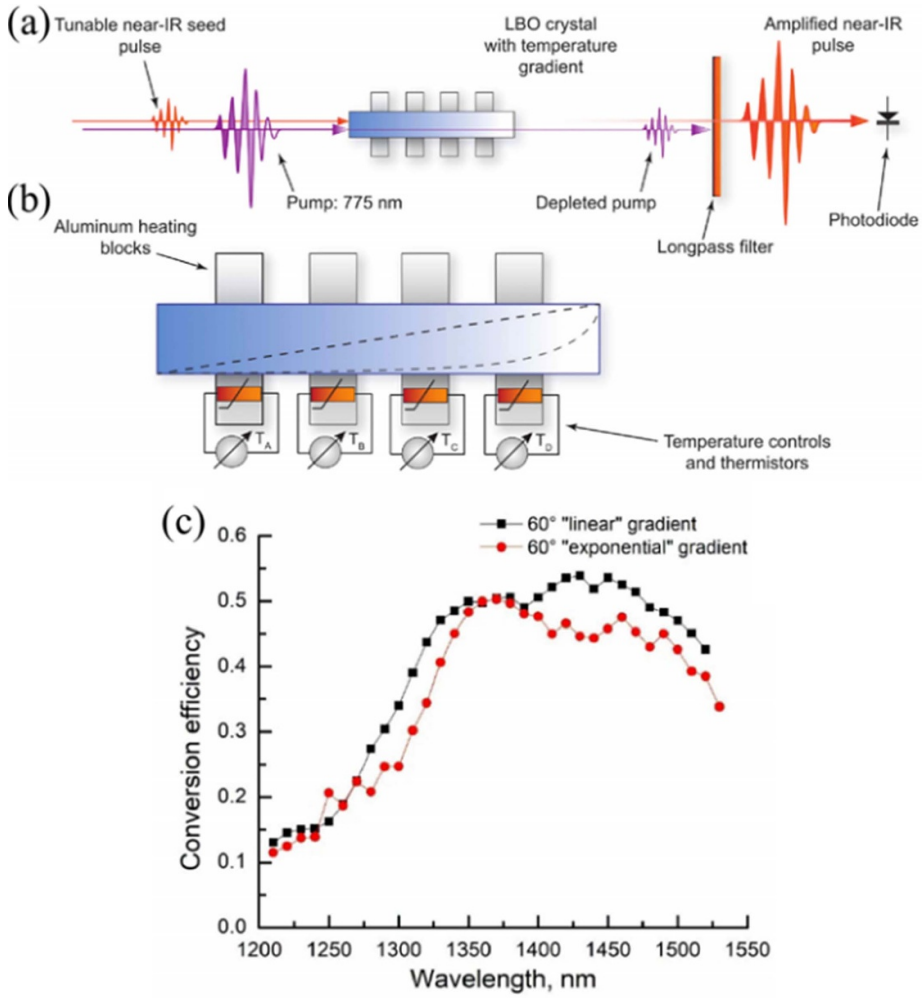

Figure 9. Adiabatic OPA with pump depletion, using temperature gradients. (a) Schematic of the experimental setup. (b) The temperature inside the crystal is controlled by heating four equidistantly-placed spots, and using thermistors positioned in direct contact with the crystal surface. (c) Measured conversion efficiency as a function of the seed center wavelength for exponential and linear adiabatic temperature gradients. Reproduced with permission from [29].

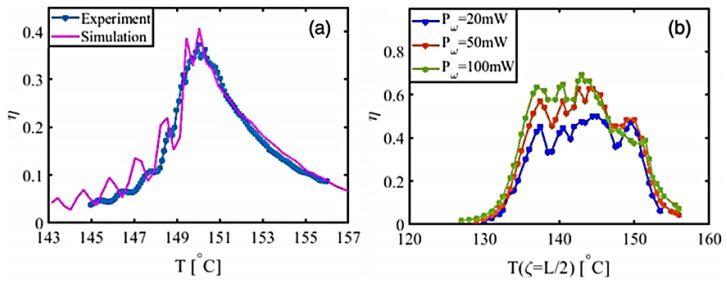

Figure 10. SHG conversion efficiency dependence on the crystal temperature (a) for a constant crystal temperature, depleted pump. The experimental (blue markers) and simulation (magenta line) results are shown. (b) Experimental results for SHG under a thermal adiabatic profile as a function of the mean crystal temperature, for three input pump intensities. Reproduced with permission from [30].

The two preceding experiments utilized the high thermal conductivity of LBO, and the significant dependence of its refractive index on temperature. Liu *et al* [31] recently introduced a new approach for realizing adiabatic frequency conversion, which utilizes another crystal property. In their method, they applied an electric gradient along a crystal (see figure 11).

Through the electro-optic effect, this field induces a gradual variation of the refractive index along the crystal, resulting in a gradual variation of the phase-mismatch. The authors chose to use a KD_2PO_4 (DKDP) crystal due its large electro-optic coefficient ($r_{63} \approx 25$ pm V^{-1}). Using a nanosecond laser, the authors were

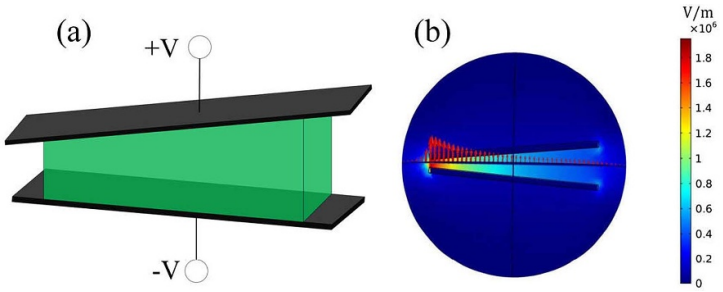

Figure 11. (a) Schematic of a nonlinear crystal sandwiched between a pair of electrode plates at an angle and (b) the distribution of the electric field intensity between the electrodes. Reproduced with permission from [31].

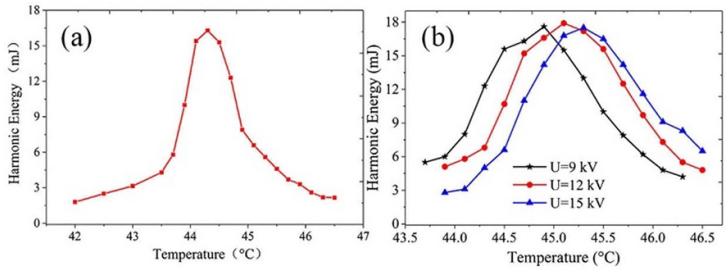

Figure 12. Dependence of second-harmonic pulse energy on crystal temperature in the (a) absence and (b) presence of an external electric field. Reproduced with permission from [32].

able to demonstrate SHG of 532 nm with 47% efficiency and a four-fold increase of the temperature acceptance bandwidth as compared to conventional birefringent phase-matching (see figure 12).

Interestingly, the crystal's aperture was very large, 6 × 10 mm, so this approach could also facilitate power-scaling. Furthermore, this method is readily applicable in other commonly-used nonlinear crystals with large electro-optic coefficients, such as $LiNbO_3$ ($r_{51} \approx 32$ pm V^{-1}) and KTP ($r_{51} \approx 7$ pm V^{-1}).

Adiabatic frequency conversion in the quasi-monochromatic regime was extremely useful in facilitating highly efficient and robust conversion of long-duration sources (either narrowband or broadband and chirped). However, due to the nonlinear nature of frequency conversion processes, the high intensity associated with compressed ultrashort pulses could be leveraged to facilitate even higher conversion efficiency. Additionally, direct frequency conversion of compressed ultrashort pulses would reduce the experimental complexity and power loss resulting from pulse-stretching. The extension of fully nonlinear adiabatic frequency conversion to the compressed ultrashort-pulse regime is reviewed in the next section.

4. Adiabatic frequency conversion with compressed ultrashort pulses in the fully-nonlinear regime

When employing compressed femtosecond pulses in adiabatic frequency conversion—an important parameter space for ultrafast sources—equation (7) is no longer valid and a model incorporating pulse propagation effects is required. In 2017, Dahan *et al* [52] published a generalized theoretical model of ultrafast adiabatic frequency conversion, including high-order dispersion and additional (parasitic) nonlinear effects, namely two-photon absorption and the Kerr effect. The authors demonstrated the validity of their theory using ultrafast adiabatic SHG, though the model is also applicable to DFG and SFG.

The dynamical equations that govern the general TWM process are [52]:

$$\frac{\partial B_{\mathrm{s}}(z,t)}{\partial z} + i\mathcal{F}^{-1}\left\{k(\omega+\omega_{\mathrm{c,s}})\,B_{\mathrm{s}}(z,\omega)\right\} = -i\chi^{(2)}(z)\,\mathcal{F}^{-1}\left\{\frac{\omega+\omega_{\mathrm{c,s}}}{cn(\omega+\omega_{\mathrm{c,s}})}\mathcal{F}\left\{B_{\mathrm{i}}(z,t)\,B_{\mathrm{p}}^{*}(z,t)\right\}\right\}$$

$$\frac{\partial B_{\mathrm{p}}(z,t)}{\partial z} + i\mathcal{F}^{-1}\left\{k(\omega+\omega_{\mathrm{c,p}})\,B_{\mathrm{p}}(z,\omega)\right\} = -i\chi^{(2)}(z)\,\mathcal{F}^{-1}\left\{\frac{\omega+\omega_{\mathrm{c,p}}}{cn(\omega+\omega_{\mathrm{c,p}})}\mathcal{F}\left\{B_{\mathrm{i}}(z,t)\,B_{\mathrm{s}}^{*}(z,t)\right\}\right\}$$

$$\frac{\partial B_{\mathrm{i}}(z,t)}{\partial z} + i\mathcal{F}^{-1}\left\{k(\omega+\omega_{\mathrm{c,i}})\,B_{\mathrm{i}}(z,\omega)\right\} = -i\chi^{(2)}(z)\,\mathcal{F}^{-1}\left\{\frac{\omega+\omega_{\mathrm{c,i}}}{cn(\omega+\omega_{\mathrm{c,i}})}\mathcal{F}\left\{B_{\mathrm{s}}(z,t)\,B_{\mathrm{p}}(z,t)\right\}\right\}, \quad (10)$$

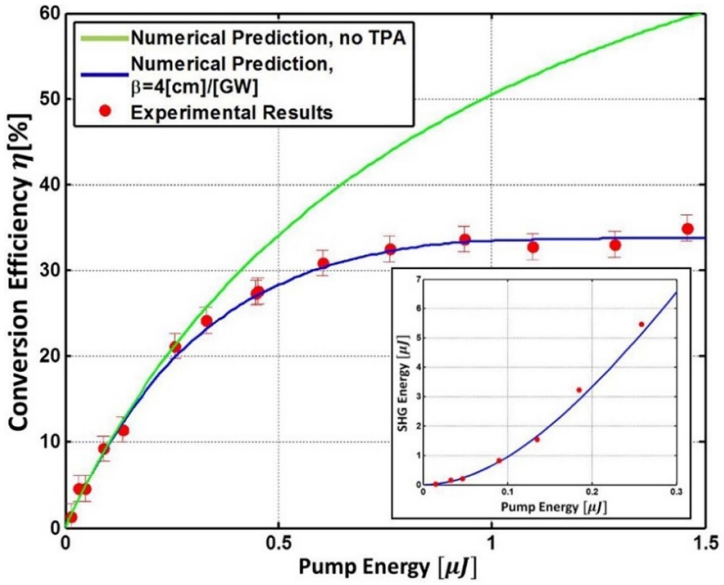

Figure 13. Conversion efficiency as a function of pump energy. Deviation between the loss-free numerical predication and experimental results can be attributed to TPA. Inset: the generated SHG pulse energy exhibits quadratic dependency on the incident pump pulse energy for low energies. Reproduced from [52]. © IOP Publishing Ltd. All rights reserved.

where $B_{s,p,i}(z,\omega) = A_{s,p,i}(z,\omega)\,e^{-ik(\omega)z}$, $k(\omega)$ is the frequency-dependent wavenumber, and $A_{s,p,i}(z,\omega)$ are the spectral amplitudes of the waves (i.e. the Fourier transform of the waves' slowly varying temporal envelopes).

The notation '$\omega+\omega_{c,j}$' is used to emphasize the broad spectral range of the waves: $\omega_{c,j}$ is the central frequency of each wave j, and ω covers the spectral range of each pulse around its center. The second term on the left side of each equation, $\mathcal{F}^{-1}\left\{k\left(\omega+\omega_{c,j}\right)B_j(z,\omega)\right\}$, accounts for the dispersion the pulses experience while propagating through the medium. The term on the right side of each equation accounts for the nonlinear interaction between the pulses.

In the case of SHG, $\omega_s = \omega_p$ is the pump and $\omega_{SHG} = 2\omega_p$ is the second harmonic. Taking into account two-photon absorption, through an intensity-dependent absorption coefficient $\alpha = \alpha_0 + \beta I$, and the Kerr effect, through an intensity-dependent refractive index $n = n_0 + n_2 I$, the following dynamic equations are obtained [52]:

$$\frac{\partial A_{SHG}(z,t)}{z} + i\mathcal{F}^{-1}\left\{k(\omega+\omega_{c,SHG})\,\mathcal{F}\left\{A_{SHG}(z,t)\right\}\right\} = -i\chi^{(2)}(z)\,\mathcal{F}^{-1}\left\{\frac{\omega+\omega_{SHG}}{cn(\omega+\omega_{SHG})}\mathcal{F}\left\{A_p^2(z,t)\right\}\right\}$$
$$-\frac{\beta}{2}I_{SHG}(z,t)\,A_{SHG}(z,t) - ik_0 n_2(\omega_{SHG})\left[I_p(z,t)+I_{SHG}(z,t)\right]A_{SHG}(z,t)$$

$$\frac{\partial A_p(z,t)}{z} + i\mathcal{F}^{-1}\left\{k\left(\omega+\omega_p\right)\mathcal{F}\left\{A_p(z,t)\right\}\right\} = -i\chi^{(2)}(z)\,\mathcal{F}^{-1}\left\{\frac{\omega+\omega_p}{cn\left(\omega+\omega_p\right)}\mathcal{F}\left\{A_{SHG}(z,t)\,A_p^*(z,t)\right\}\right\}$$
$$-ik_0 n_2\left(\omega_p\right)\left[I_p(z,t)+I_{SHG}(z,t)\right]A_p(z,t), \qquad (11)$$

where $I_p(z,t) = \frac{|A_p(z,t)|^2 n_p}{\eta_0}$ and $I_{SHG}(z,t) = \frac{|A_{SHG}(z,t)|^2 n_{SHG}}{\eta_0}$.

The analysis is performed by numerical simulations using the split-step Fourier method. Figure 13 compares the theoretical prediction of conversion efficiency with experimental results, showing excellent correspondence.

Later work by the same group achieved highly-efficient, robust, broadband and spectrally-flat conversion over a wide bandwidth of 35 nm [20]. This allows, as predicted theoretically and realized experimentally, pulse shaping and phase control of broadband second-harmonic pulses (see figure 14). We would like to note that in contrary to the adiabatic DFG process in the undepleted pump approximation, which allow one-to-one spectral phase and amplitude conversion, in adiabatic SHG the control by the spectral phase is limited.

The shaping of the near-IR pump pulse was carried out using an SLM in a 4f configuration. The pulse shape was successfully transferred to the second-harmonic vis the adiabatic frequency conversion. This work

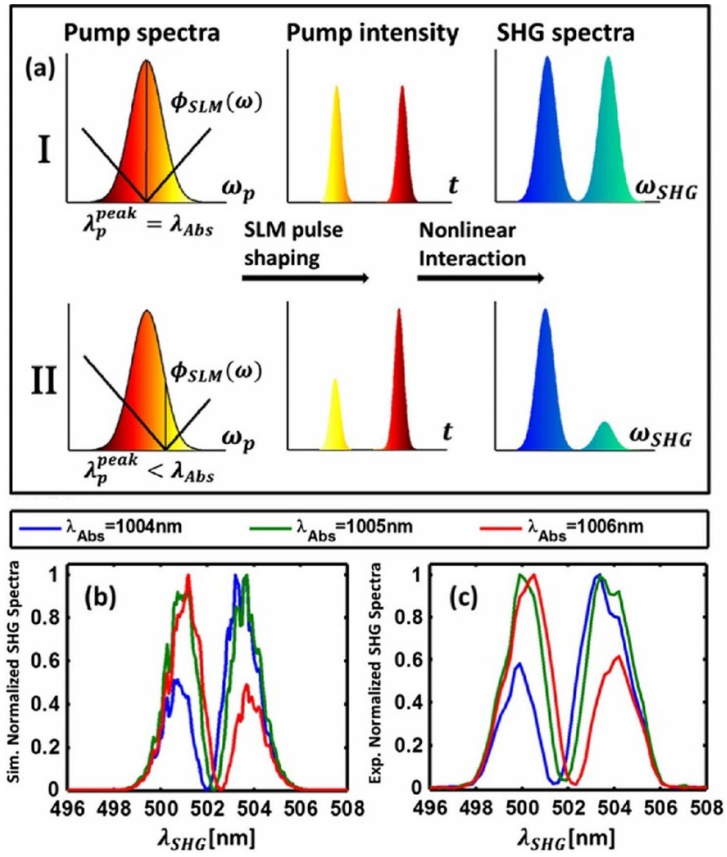

Figure 14. Absolute phase effects of the SHG pulse for different ω_{Abs}, the central absolute phase frequency. (a) Illustration of absolute phase concept Here, using a pulse shaper, an absolute spectral phase was applied at the center of the pump spectra (left scheme), dividing temporally the pump pulse into two pulses (center scheme). The separated pulses have been converted efficiently to their SHG (right scheme). (b) Simulated normalized SHG spectra. (c) Experimental normalized SHG spectra. Reproduced with permission from [20].

serves as a proof of concept for other pulse-shaping applications for spectroscopy and imaging. The significance of working with short pulses is highlighted in this experiment by the high conversion efficiency that was achieved, even when pumping directly with low-energy (10–30 nJ) Ti:Sapphire oscillator pulses. More than 50% conversion efficiency was obtained for 70 fs pulses (17.5 nm FWHM transform-limited) at 80 MHz repetition rate.

5. Cascaded adiabatic frequency conversion for high repetition rate ultrafast sources

Cascading adiabatic frequency conversion processes can increase their spectral reach, as well as introduce new capabilities. Using nanosecond pulses, the cascading of processes was experimentally demonstrated to facilitate tunable upconversion [59] and conversion through a dark intermediate frequency [60, 61]. Theory and simulation predict that such schemes will enable novel optical switching techniques. Additionally, cascaded conversion of spectrally-close sources was shown to have the potential to generate frequency combs [62]. These long-pulse ($\gg$1 ps) works were previously reviewed in detail [28]. Here we focus on newer applications of cascaded adiabatic frequency conversion in the ultrafast domain. In particular, these have been shown to facilitate scaling of pulse repetition rate.

Increasing the pulse repetition rate of ultrafast laser sources is important for several types of applications. Higher repetition rate leads to higher average power, which is necessary for improving signal-to-noise ratio in a given measurement time. Some applications, such as photoemission spectroscopy [63] and reaction microscopy [64], can only make use of limited pulse energy (e.g. due to space charge effects in photoemission spectroscopy). In those applications, scaling up the pulse repetition rate is the only way to improve SNR. Also, having higher average power is required for long-sought attosecond pump-attosecond probe experiments, which are currently not feasible with tabletop systems due to average power limitations. Other existing and future applications, which utilize frequency combs, require high repetition rates in order to be able to easily access each comb tooth individually. These include astrophysical spectrograph calibration and future optical communication systems.

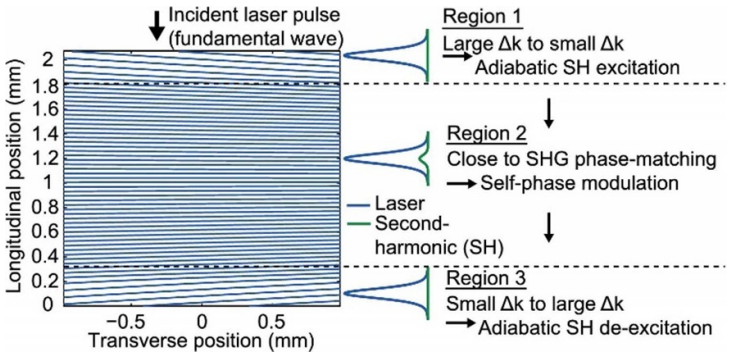

Figure 15. Illustration of the cascaded adiabatic SHG QPM design implemented in MgO:$LiNbO_3$ (see text for details). To the right of the QPM pattern, the time-dependent intensity of the laser and its SH are illustrated, indicating the small SH intensity in regions 1 and 3, and the moderate intensity in region 2. Reproduced with permission from [69].

Most commonly, ultrafast mode-locked lasers operate at a repetition rate of 50–100 MHz. In Ti:Sapphire amplifiers, it has been very common to sample these pulses at ∼1 kHz before amplification, in order to reduce thermal load and avoid damage by bringing the amplified average power down to the Watt level. However, maturing Yb:fiber and Yb:thin-disk technology has demonstrated amplification to kW average power levels at full repetition rates [65–68]. Therefore, amplifying very high repetition rate lasers to very high average power is now at hand.

Scaling the repetition rate of ultrafast lasers is challenging, as it requires the laser cavity to be very short. In a smaller cavity it is more difficult to integrate elements that will stabilize the mode-locking process, such as dispersion tuning elements (e.g. grating pairs). This issue is compounded by the fact that a higher repetition rate means lower pulse energy (for the same average power), making it more difficult to facilitate self-starting, stable mode-locking. A particular source of concern are Q-switching instabilities, as they can result in component damage.

Phillips *et al* [69] addressed this problem by using cascaded adiabatic SHG to facilitate soliton formation in a SESAM mode-locked laser, operating at a repetition rate of up to 544 MHz. In their experiment, the cavity of a diode-pumped Yb:$CaAlGdO_4$ laser contained an adiabatically poled MgO:$LiNbO_3$ crystal. This crystal was designed to facilitate a large and negative effective nonlinear refractive index, $n_2 \approx -1.5 \times 10^{-5}$ cm^2 GW^{-1} through phase-mismatched SHG. This feature facilitated soliton formation at relatively low intensities, bringing about several improvements to the laser operation. First, the laser's mode-locking was self-starting. Second, the negative n_2 works with the normal dispersion of the other cavity components to facilitate soliton formation, so that additional dispersion control elements are not required and the cavity length can be kept short to facilitate a high repetition rate. Third, the crystal introduced a small nonlinear loss, which helps to suppress Q-switching.

In order to achieve the large and negative n_2, the crystal was designed to have three sections (see figure 15). The first section was adiabatically chirped from a large phase-mismatch to a small, but non-zero, phase-mismatch. The second section was periodically poled to keep this small phase-mismatch constant. The third section was a mirror image of the first, bringing the phase-mismatch back to a high value. In the first section, a small amount of SH is generated. The back-and-forth exchange of energy between the SH and FH (fundamental harmonic) in the second section is responsible for the large negative effective n_2 [70]. In the third section, the remaining SH is converted back to the FH. Using adiabatic chirping for the first and third sections is important since it keeps the system in an eigenstate. This means that the third section is able to perfectly and robustly reverse the effect of the first section, eliminating the SH. This is in contrast to using a crystal with a fixed phase-mismatch, where residual SH means high losses that destabilize the mode-locked laser.

Using this approach, the laser could produce 100 fs pulses with 740 mW average power at 540 MHz repetition rate, or 149 fs pulses with 1.45 W average power at 544 MHz repetition rate.

In a following work [71], the same group was able to scale their laser's repetition rate to 10.6 GHz, while maintaining 1.2 W of average power and 166 fs pulses. This was achieved by taking advantage of the strong nonlinear self-defocusing afforded by the negative effective n_2 of the MgO:$LiNbO_3$ crystal. The self-defocusing allowed the cavity to be very compact (see figure 16), with small beam waists in the gain medium and on the SESAM, since the defocusing would prevent high-intensity light from damaging the optical components (such damage results from the high intensity associated with Q-switching instabilities).

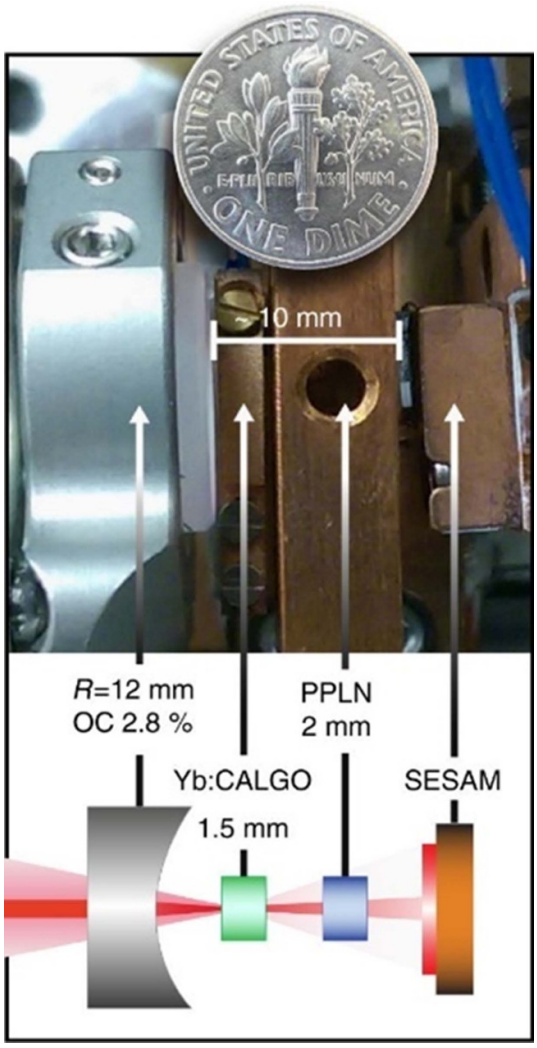

Figure 16. Schematic and photo of the 10 GHz Yb:CALGO laser cavity, which is stabilized by cascaded adiabatic SHG implemented in $MgO:LiNbO_3$ (labeled PPLN by mistake in the original publication [71]). Reproduced from [71]. CC BY 4.0.

In fact, the defocusing effect worked to reduce the overlap between the cavity mode and pump beam, thereby limiting the maximum attainable laser gain, and correspondingly limit the maximum intracavity intensity.

Cascaded adiabatic frequency conversion has also been utilized for efficient generation of a UV frequency comb. Liu *et al* [34] cascaded $\chi^{(3)}$-based spectral broadening with multiple adiabatic SHG processes to generate an UV frequency comb spanning 360–425 nm. This was accomplished with a chip-scale platform: adiabatically tapered AlN waveguides (see figure 17). A 100 fs near-IR laser, with 80 MHz pulse repetition rate, was incident onto the tapered waveguide structure. Since AlN has high $\chi^{(3)}$, the pulse experienced spectral broadening due to SPM, eventually spanning 650–900 nm. The broadening process was cascaded with adiabatic SFG and SHG processes in eight chirped waveguide sections. A single tapered waveguide of the required length (5 mm) and width (0.3–0.5 μm) proved challenging to fabricate, motivating the choice of multiple tapered waveguide sections of varying length (450–800 μm). Each tapered waveguide section facilitated the upconversion of a different part of the broad near-IR spectrum, resulting in a gap-free UV comb. The high coherence of the UV comb was verified experimentally by beating it with a CW laser with a 50 kHz linewidth. This experiment highlights the usefulness of ultrafast adiabatic frequency conversion at high pulse repetition rate.

6. Adiabatic FWM

Quadratic media as a platform for adiabatic frequency conversion has two primary advantages. First, the value of $\chi^{(2)}$ is large in common media, allowing high conversion efficiency in a short length. Second, QPM may be implemented effectively through ferroelectric domain poling in several of the best materials available for frequency conversion. However, the absence of $\chi^{(2)}$ in centrosymmetric media prevents applications of

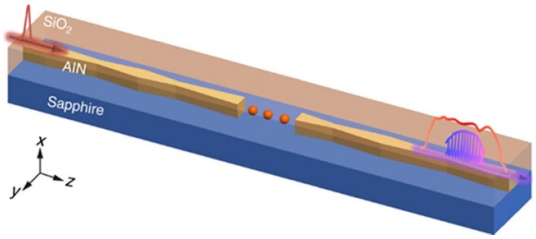

Figure 17. Illustration of the chirp-modulated taper waveguide based on single-crystalline AlN thin films. The red solid spheres indicate omitted waveguide segments. Reproduced from [34]. CC BY 4.0.

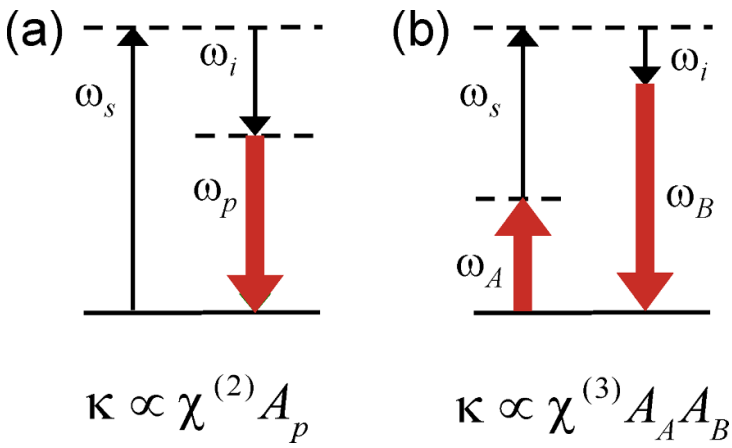

Figure 18. Frequency up/down-conversion schemes for (a) quadratic nonlinear platforms by sum- and difference-frequency generation and (b) cubic nonlinear platforms by Bragg scattering FWM.

adiabatic TWM in many important optical devices, including two of the most important waveguide platforms: fiber optics and integrated silicon photonics.

Nonlinear frequency conversion applications of many forms take place through the cubic nonlinear susceptibility by FWM, including parametric amplification, frequency up- and downconversion, and third harmonic generation. These applications generally suffer from the same limitations observed in TWM applications: limited phase-matching bandwidth, bandwidth-efficiency trade-offs, and sensitivity of the conversion efficiency to pump and seed power due to the existence of back-conversion. Waveguides often play a crucial role in frequency conversion applications in cubic media. The property of perturbative nonlinear optics that $\left|\chi^{(3)}E_{\text{applied}}\right| \ll \left|\chi^{(2)}\right|$ means that generally longer lengths are needed in cubic media compared to quadratic media for efficient nonlinear conversion. The long nonlinear interaction lengths enabled by waveguides thus become essential. On the other hand, a longer interaction length results in a narrower phase-matching bandwidth, and schemes that can broaden the phase-matching bandwidth could therefore have broad impact for applications of FWM frequency conversion.

Bahar *et al* [54] published the first investigation of adiabatic FWM frequency conversion, establishing the theory of adiabatic frequency up- and down-conversion via Bragg-scattering FWM (BS FWM), which possesses the dynamics of RAP in direct analogy to adiabatic sum- and difference-frequency generation in quadratic nonlinear media. Figure 18 compares the two processes. In both cases, the goal is a full photon population inversion from signal to idler, or vice-versa. In the FWM case, there are two pump fields with greater photon number than signal and idler, with amplitudes labeled A_{A} and A_{B}. The adiabatic condition (equation (3)) is still valid. However, the nonlinear coupling coefficient κ is now proportional to $\chi^{(3)}A_{\text{A}}A_{\text{B}}$, and the wave-vector mismatch is modified by phase shifts due to self- and cross-phase modulation imparted by the pump waves, $\Delta k = k_{\text{A}} + k_{\text{s}} - k_{\text{B}} - k_{\text{i}} + \Delta k_{\text{PM}}$, where Δk_{PM} is a linear function of the pump intensities.

Employing numerical models, Bahar *et al* [54] predicted broadband downconversion by adiabatic BS FWM in both step-index fibers and silicon waveguides, utilizing a longitudinal variation of the waveguide dimension to achieve the sweep $\Delta k(z)$ needed to satisfy the adiabatic condition. In an example silicon photonic device, a chirped modulation of a strip waveguide's width along the propagation direction allowed downconversion of a 70 nm bandwidth, centered at 1.68 μm to 1.82 μm, with a photon conversion efficiency

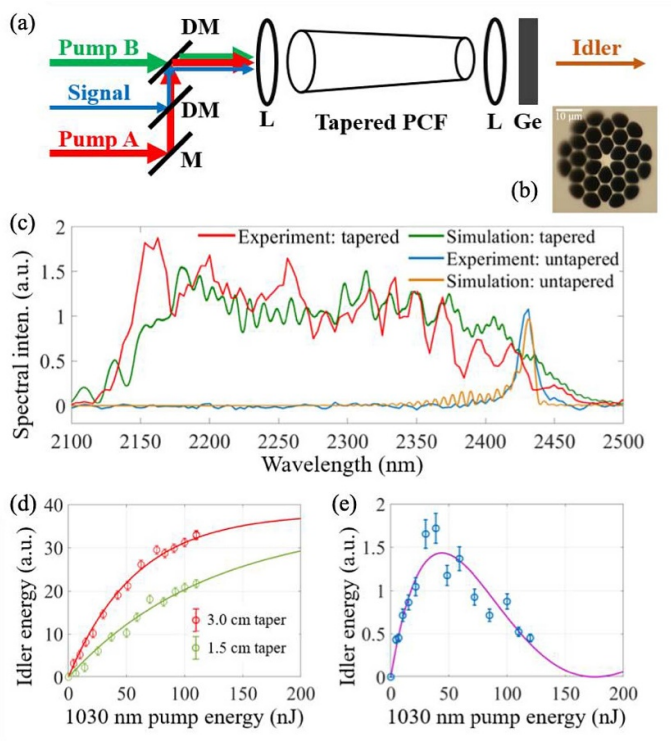

Figure 19. Experimental demonstration of adiabatic FWM in a tapered photonic crystal fiber (PCF). (a) Schematic of the experiment. (b) Microscope image of the fiber cross section. (c) Idler power spectra from tapered fiber (adiabatic) and untapered fiber (nonadiabatic) experiments and corresponding numerical predictions. The dependence of conversion efficiency on pump power for the tapered fiber (d) and untapered fiber (e) experiments demonstrates the dynamics of RAP and Rabi-flopping, respectively. Reprinted figure with permission from [33], Copyright 2020 by the American Physical Society.

greater than 90%. The pump pulses at 2.0 μm and 2.2 μm wavelength required only 10 pJ energy. In an example fiber device, a fluoride step-index fiber was proposed and investigated, using a core taper to achieve the needed sweep of $\Delta k(z)$. Maximizing conversion bandwidth by choosing a fiber with zero-dispersion wavelength lying between pairs of the four interacting waves, λ_A and λ_i to one side and λ_B and λ_s to the other, adiabatic phase matching could be achieved for downconversion of a 1.36–1.44 μm signal to a 4.2–5.2 μm idler. The modeled fiber had a core radius taper from 4.5 μm to 3.55 μm over a length of 5 cm. The ~10 ps pump pulses were at the Tm:fiber wavelength of 2.0 μm and its second harmonic at 1.0 μm, and had 100 kW peak power. The predicted 5 nJ idler output pulse energy with <50 fs transform-limited duration at 4.7 μm central wavelength thus represents a potential route to a powerful ultrafast all-fiber based system for the mid-IR in this spectral range.

Ding *et al* recently completed the first experimental realization of an optical fiber adiabatic frequency conversion device [33]. In a 3 cm highly nonlinear PCF with a 4.2 μm to 3.6 μm core diameter taper, 1 nJ, sub-100 fs near-IR pulses spanning 696–723 nm were efficiently converted to mid-IR wavelengths spanning 2.15–2.43 μm (supporting a 75 fs pulse) by adiabatic BS FWM in the presence of a 1030 nm wavelength, 3 ps, 110 nJ pump 'A' and a 515 nm, 2 ps, 24 nJ pump 'B' (figures 19(a)–(c)). On average, a 70% signal to idler photon conversion efficiency was obtained. In comparison, an untapered 3 cm fiber of 4.2 μm core diameter produced a 25× narrower idler bandwidth. Tapered fibers (figure 19(d)) produced the expected robust, asymptotic approach to full conversion characteristic of RAP while untapered fibers (figure 19(e)) illustrated the back-conversion characteristic of Rabi-flopping dynamics.

This first realization of RAP in optical FWM in an optical fiber suggests that fiber platforms more suitable for intense ultrafast sources may also be realized. In particular, adiabatic frequency conversion in hollow waveguides presents an intriguing platform for producing ultrafast sources used to drive strong-field science, as the gas core can possess both a high damage threshold and broad spectral transmission range. A fiber with a wide core diameter could thus accommodate high energy pulses with wide signal and idler bandwidths spanning disparate spectral ranges.

Ding *et al* performed a numerical investigation of octave-spanning downconversion by adiabatic BS FWM in a tapered AR HCF filled with Ar gas [32], showing that 10 μJ, near-single-cycle pulses might be generated in the mid-IR. Figure 20 illustrates the fiber design for pump wavelengths corresponding to an Yb:YAG laser (1030 nm) and its second harmonic (515 nm), a broadband near-IR signal (770–860 nm), and

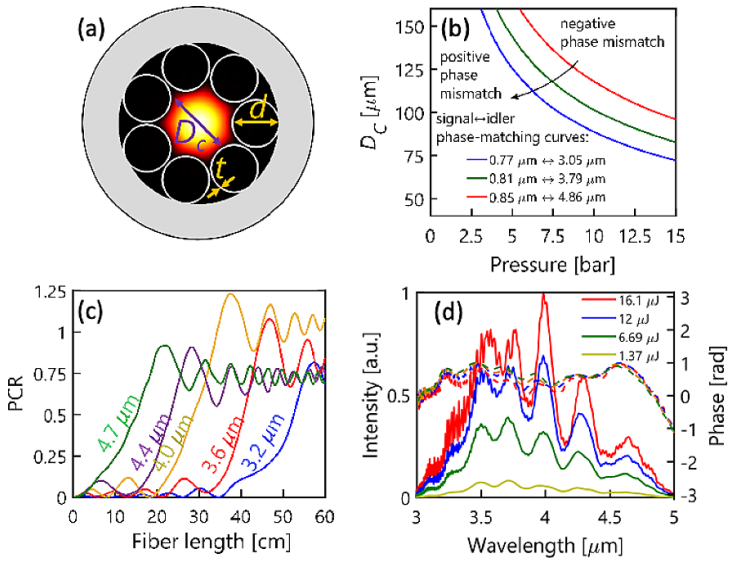

Figure 20. Numerical study of adiabatic FWM in an anti-resonant hollow core fiber (AR HCF). (a) Schematic of the fiber cross-section. (b) Phase-matching curves for varying core diameter, D_C, and Ar gas pressure, with arrow indicating the longitudinal variation of the simulated fiber design. (c) Longitudinal evolution of the photon conversion ratio (PCR) for signal to idler conversion. (d) Idler power spectrum corresponding to several final idler pulse energies obtained by variation of the input signal energy. Reproduced with permission from [32].

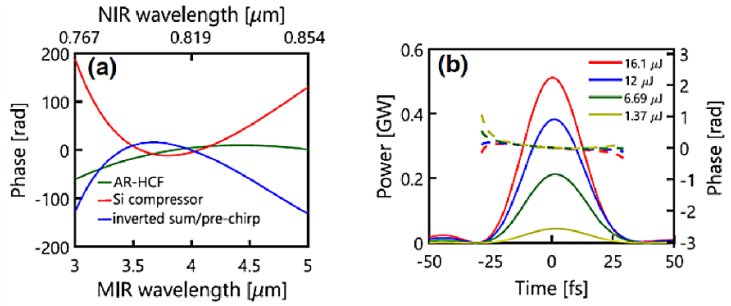

Figure 21. Transform-limited mid-IR pulse compression and shaping. (a) Phase accumulated in AR-HCF, in 5.2 cm of bulk Si, and their inverted sums. (b) Temporal intensity (solid) and phase (dashed) profiles of compressed mid-IR pulses at different output energies. Reproduced with permission from [32].

a generated mid-IR idler covering most of an octave (3–5 μm). To investigate a physically realizable design, the authors limited the taper ratio (covering a 130–110 μm core diameter over a 60 cm long fiber length) and utilized a gas pressure gradient to increase the overall variation in $\Delta k(z)$. This also imparted a longitudinal change in the nonlinear coupling coefficient, $\kappa(z)$, which thus also played a role in the fulfillment of the adiabatic condition (equation (3)). Figure 20(c) illustrates characteristic adiabatic evolution for several idler frequencies. Conversion efficiencies greater than one indicate the presence of a small degree of a parasitic FWM process, which acts to amplify some idler frequencies. The predicted broad mid-IR idler spectrum, covering 3–5 μm (figure 20(d)), can be boosted to 12 μJ by increasing the signal pulse energy before this parasitic process becomes strong enough to cause strong spectral modulation. The authors found that for obtained idler pulse energies of up to 16 μJ, the idler spectral phase does not vary with the signal energy, indicating a linear spectral transfer function. Moreover, for an architecture in which the input signal band and pump 'B' are derived from pump 'A' by white light generation and SHG, respectively, the process is expected to produce an idler with passively stable CEP.

Figure 21 summarizes pulse propagation simulations showing that a 27 fs pulse (compared to a 26 fs transform limited duration) spanning 3–5 microns (around 2–3 optical cycles) can be obtained from the AR-HCF AFWM device by pre-shaping the phase of the near-IR signal pulse prior to conversion [32], using only GVD and TOD compensation. The obtained pulse shape is independent of the signal energy in the range shown, showing again that the device has a linear phase transfer function. This is an example of how the adiabatic down-conversion method can simplify dispersion management for a very broadband pulse, independent of pulse energy.

The results presented in this section show that adiabatic downconversion by FWM in hollow optical fibers preserves the pulse phase, allowing pre-conversion pulse shaping that can simplify dispersion management for a very broadband pulse and that is independent of the pulse energy. This section also presents a promising high-energy pulse generation scheme for generation of a passively stabilized CEP in a near-octave-spanning down-converted pulse.

7. Attosecond science and HHG

Progress in attosecond science depends strongly on developments in ultrafast laser technology. Ultrafast laser sources are required to drive the strong-field interactions that open a window into the domain of attosecond physical dynamics and that are used to generate attosecond pulses for probing other material systems [1, 2].

For many years, the workhorse of the field has been the short-pulse, high-energy, near-IR Ti:Sapphire laser. Extending its properties to other spectral ranges, in particular the mid-IR, remains an active field of research. Moreover, attosecond domain applications have motivated the development of ultrafast source technology with unusual characteristics, such as coherent multi-spectral sources, single- and few-cycle pulses with CEP stability and control, and the shaping of ultrabroadband light pulses possessing non-sinusoidal waveforms. Such applications include shaping the trajectories of ionized electrons, HHG spectroscopy of low-ionization-potential biomolecules, and the generation of x-ray femtosecond and attosecond pulses [3–10].

Ultrafast adiabatic frequency conversion delivers a number of new source capabilities that can address the demands for advancing attosecond and HHG research.

First, attosecond pump-probe experiments would ideally use attosecond pulses for both pump and probes. However, existing attosecond pulse sources generally provide too low pulse energy and flux to be used for such purposes, so currently researchers carry out pump-probe experiments combining femtosecond and attosecond pulses. The influence of the femtosecond pulse makes interpretation of observations significantly more difficult. The attosecond pulse flux is strongly limited by Ti:Sapphire laser technology, where it is very difficult to maintain adequately high pulse energy while pushing the pulse repetition rate (and hence the flux) beyond the kHz range. New laser technology is emerging that can provide relatively high pulse energy (>100 μJ) at MHz repetition rates. As mentioned above, these lasers are based on Yb-doped media, such as Yb:fiber or Yb:thin-disk, which produce near-IR light around 1 μm wavelength. Still, pulse energy at high repetition rates remains low as compared to low-repetition rate ($\ll$1 MHz) systems that reach 100 mJ in common tabletop systems (including both Ti:Sapphire [72] and Yb:thin-disk [73]). This issue is compounded by the narrower gain bandwidth of Yb-doped media (about ¼ of the gain bandwidth of Ti:Sapphire), which makes it necessary to introduce additional spectrum-broadening nonlinear processes in order to facilitate further pulse-compression. For high repetition rate systems with pulse energy well below 1 mJ, significant nonlinear broadening requires strong spatial confinement (tight focusing or guiding structures), resulting in spectral inhomogeneity across the beam or significant loss of power [74–76], facilitating shorter yet less-energetic pulses. Having lower pulse energy makes frequency conversion of these near-IR sources challenging, as nonlinear optical processes depend strongly on peak power. Moreover, all laser sources suffer deleterious losses when frequency conversion is used to access other wavelengths. Thus, while the efficiency of the frequency conversion step is a crucial factor for any repetition rate, it is even more so for high repetition rate attosecond pulse sources needed for photoemission and photo-fragmentation studies, where the number of emitted particles per laser pulse must be limited (in both existing attosecond-femtosecond pump-probe schemes and any attosecond pump-probe scheme that may become possible in the future). For example, in time and angle resolved photoemission spectroscopy and in cold target recoil ion momentum spectroscopy, space-charge effects, resulting from the interaction between multiple emitted electrons or ions, distort the spectroscopic information. Often in these studies, the required attosecond pulse energy is moderate while average flux is the limiting factor [77–80].

Second, attosecond pulse generation and attosecond phenomena depend on the temporal shape of the pulses that drive them (e.g. in HHG [1] or attochemistry [81]). While low-loss pulse-shaping of near-IR light is straightforward, pulse-shaping of mid-IR or UV light can be challenging, especially with low losses. In the past decade of attosecond science research, particular attention has been dedicated to the generation of precisely shaped and CEP-stable greater-than-octave-spanning pulses. Such so-called ‘waveform control’ may benefit a number of strong-field applications where the shaping of a waveform over a single optical cycle is desired. These benefits include boosting HHG (and attosecond pulse) photon energy, efficiency, or both [82–84]. The last decade has seen numerous efforts to create such pulses for strong-field physics by means of coherent pulse synthesis [85]. One prototypical example is the splitting of multiple bands of a multiple-octave hollow-core fiber compressor spectrum for separate compression by double-chirped-mirror

pairs followed by coherent recombination [15]. Another example is the separate amplification of multiple spectral bands by OPA or OPCPA followed by coherent recombination [16, 17].

Third, as explained above, scaling the frequency of attosecond pulses into the x-ray regime requires scaling the frequency of suitable driving lasers into the mid-IR regime, while achieving the necessary pulse energy. To date, the most promising approach for this purpose has been OPA. Power scaling is achieved by cascading multiple OPAs [47, 86]. Each OPA stage introduces additional noise into the output pulse. Beam-pointing instabilities increase with each stage, and appear as yet additional noise at the mid-IR output. When such a mid-IR source is used to generated attosecond pulses or drive other strong-field processes, the source's noise is amplified by the highly nonlinear processes involved, such as multi-photon and tunneling ionization. Consequently, more averaging is necessary to reach useful SNR, and in some cases the averaging time can become prohibitive. Finally, OPA and DFG are inefficient processes in which a significant fraction of the pump light remains unconverted.

Ultrafast adiabatic frequency conversion can address all of these challenges. It facilitates efficient, broadband and coherent (maintaining CEP stability) frequency conversion, which can be combined with pulse-shaping of the output with no additional losses. Achieving high conversion efficiency without compromise for bandwidth compensates for the lower pulse energies of novel high repetition rate Yb-doped laser sources. Additionally, the high efficiency of adiabatic OPA reduces the necessary number of amplification stages, further improving the noise characteristics of the mid-IR output, and can provide a higher final energy. Where waveform control is desired, octave-spanning spectra from adiabatic downconversion processes may allow a convenient alternative to coherent pulse synthesis. The mid-IR pulses generated in Krogen *et al* by adiabatic DFG in PPLN were already demonstrated with arbitrary pulse shaping over a 1.3-octave mid-IR bandwidth at the microjoule pulse energy level [19]. By mid-IR pulse generation via adiabatic BS FWM in a tapered AR HCF, Ding *et al* [32] predict near-octave spanning bandwidth above 10 μJ with a close to linear transfer of phase and amplitude, thus allowing precise pulse shaping by pre-shaping prior to conversion. Both techniques should allow for passive idler CEP stabilization by deriving the signal and pump waves from a common laser, and thus should be extendable to arbitrary waveform shaping. The pulse energies of these sources are already in the range where they can be useful for HHG in solid materials, where there has been much interest in mid-IR driver frequencies, single-cycle driver pulse durations and pulse shaping capability to produce isolated attosecond bursts [87, 88]. Adiabatic FWM in large-core gas-filled hollow capillary fibers may allow the technique to be further scaled in the future to the sub-millijoule energy regime and beyond, where the generated pulses could be used for strong-field applications in gas media. Moreover, the future exploration of ultrafast adiabatic FWM in the fully nonlinear regime could help to identify source architectures for shapeable octave-spanning sources at high energies where efficient conversion of the pump wave is desired.

The average power scalability of adiabatic frequency conversion has recently been demonstrated by Rozenberg and Arie [30], as detailed in section 3. Two major limitations for such scaling are laser damage and local heating that leads to inhomogeneity and lowered efficiency [89]. The former is restrictive where the crystal aperture is small (usually $0.5-1$ mm), which is necessary for implementing electric field poling. The latter is constrained by the crystal's thermal conductivity. Rozenberg and Arie's use of temperature gradient made it possible to utilize a large-aperture (5×5 mm) LBO crystal for adiabatic SHG. LBO possesses one of the highest laser damage thresholds among all nonlinear crystals and a high thermal conductivity of 3.5 W m^{-1} K^{-1}, but is not amenable to poling. The large aperture means that high average-power lasers can be more loosely focused such that the peak intensity is still below the crystal's damage threshold.

Ultrafast adiabatic frequency conversion can also open new opportunities for attosecond pulse generation that is not based on the conventional scheme of infrared-driven HHG in neutral atoms. It can facilitate efficient, broadband and coherent frequency conversion into the ultraviolet as well. By delivering more powerful ultraviolet sources, it can improve the performance of the abovementioned method [10], where an ultrafast ultraviolet laser drives ionization followed by HHG. For example, it could enable using this method with higher repetition rate and more modest pulse energies. Additionally, Yb-doped sources have been shown to generate very high flux extreme UV power by cascading perturbative nonlinear processes, rather than HHG, or with HHG. In one case, the second, third or fourth harmonic of a 166 kHz Yb:fiber laser were used to drive HHG in gases, delivering extreme UV light (down to a wavelength of 34 nm) [82]. The efficiency of the TWM processes in this cascade could be further improved by utilizing adiabatic frequency conversion. This improvement would directly translate into higher attosecond pulse flux.

8. Summary and outlook

In this article, we reviewed the ultrafast adiabatic frequency conversion method and its applications. We focused on this method's demonstrated and expected contributions to ultrafast technology that underlies attosecond science, strong-field physics, HHG spectroscopy and (multidimensional) mid-IR spectroscopy.

Adiabatic frequency conversion is facilitated by a gradual variation of system parameter, which makes the system state follow a correspondingly varying eigenstate. The main attributes of ultrafast adiabatic frequency conversion are the high conversion efficiency it delivers over a broad spectral range, and the fact that it is inherently coherent. These two properties make this method capable of efficiently transferring the properties of excellent ultrafast near-IR sources into spectral ranges where such properties are difficult to achieve. One example of particular interest to attosecond science is the mid-IR spectral range, where source improvements are expected to open new avenues of exploration. Such improvements include increasing pulse energy and average power (via repetition rate scaling), decreasing pulse duration and improving pulse-shaping capabilities spanning over an octave.

In section 1, we reviewed common (non-adiabatic) broadband frequency conversion methods. They all share a bandwidth-efficiency trade-off. We also provided a historical review of the development of adiabatic frequency conversion, which effectively resolves the trade-off. (More detailed information on early work can be found in Suchowski *et al* [28]). This method was gradually generalized, starting from quasi-monochromatic operation in the undepleted pump regime [27], and reaching short-pulse operation in the fully nonlinear (depleted pump) regime [52]. We also introduced the technical methods used to implement adiabatic frequency conversion: chirped electric-field poling, temperature gradient [29], electric field gradient [31], gas pressure gradient [32], and waveguide width variation [33, 34]. Interestingly, some of these are dynamic, allowing *in situ* optimization.

In section 2, we provided a basic introduction to the concept of frequency conversion—its principal physical origins and the requirement of phase-matching. Next, we briefly reviewed adiabatic frequency conversion under the undepleted pump approximation (for a more detailed review see [28]). The adiabaticity criterion was discussed and the unique challenges of broadband processes, GVM and GVD, were presented as well, along with the sufficient conditions to cope with them. We touched on a few publications that experimentally demonstrated important achievements with ultrafast adiabatic frequency conversion in this regime of operation. These included efficient, broadband and pulse-shape-preserving conversion of ultrafast near-IR lasers to the mid-IR all the way to the extreme of single-cycle duration with arbitrary pulse shaping capability.

In section 3, the fully-nonlinear (depleted pump) regime of adiabatic frequency conversion was reviewed. We provided an outline of the theoretical model, where additional details and connection to other models are given elsewhere [28]. We mentioned experimental demonstrations with ultrafast sources. These included highly-efficient SHG and OPA of near-IR ultrafast pulses. We also devoted attention to an experiment carried out with nanosecond pulses [30], since it shows one way to scale up the average-power handling capabilities of ultrafast adiabatic frequency conversion.

Section 4 reviews a recent development in the field: the generalization of ultrafast adiabatic frequency conversion to operation where all interacting pulses are ultrashort and have comparable intensities [52]. The theoretical model for this scheme includes additional nonlinear effects (two-photon absorption and the Kerr effect). The significance of these effects for short-pulse conversion is shown experimentally, together with demonstrations of highly-efficient SHG. Another experiment [20] shows efficient and shape-preserving conversion of ultrashort (and/or shaped) near-IR pulses to the visible range.

In section 5, the concept of cascaded adiabatic frequency conversion was presented along with a few interesting experimental realizations facilitating high pulse-repetition-rate ultrafast lasers. One group cascaded adiabatic processes for the purpose of achieving stable mode-locking at very high repetition rates, exceeding 10 GHz [71]. Another experiment demonstrated the generation of a gap-free UV frequency comb [34].

In section 6 we reviewed the very recent extension of adiabatic frequency conversion to FWM processes [32, 33, 54]. This approach immensely broadens the landscape of adiabatic frequency conversion as it can in principle be applied in any transparent media. We paid particular attention to waveguides. On the one hand, implementation with chip-scale integrated photonics waveguides and step-index fibers promises extension to very low pulse energies without loss of efficiency [54]. On the other hand, gas-filled hollow core fibers can handle very high pulse energies, promising significant energy scaling of generated ultrafast pulses, e.g. in the mid-IR [32]. We mentioned a very recent experiment utilizing a tapered-core PCF, where 70% photon conversion efficiency with nJ-level femtosecond pulses was demonstrated [33]. Numerical simulations predict shape-preserving adiabatic FWM to scale beyond 10 μJ pulse energy [32].

In section 7 we explained how ultrafast adiabatic frequency conversion rises to meet many technological challenges facing attosecond science, HHG and other related strong-field applications. Adiabatic frequency conversion can efficiently transfer the strengths of ultrafast near-IR sources to other spectral bands, in particular the mid-IR, including shaped pulses [19, 20]. Furthermore, the highly-efficient nature of this method bodes well with novel high average power, high repetition-rate sources, where a lower pulse energy often limits the conversion efficiency [20]. Altogether, these properties mean new domains of control over strong-field interactions, better access to ultrafast processes in large (bio)molecules, higher attosecond pulse flux for pump-probe experiments, and extension of ultrafast techniques to the x-ray spectral range. Additionally, we summarized recent advances in extreme UV and x-ray generation, which are based on cascading TWM and HHG processes [82] or driving an HHG in an ionized medium [10]. We proposed adiabatic frequency conversion as a means to enhance these approaches by facilitating efficient FWM or generating high-power UV driving lasers.

In conclusion, ultrafast adiabatic frequency conversion is a powerful, flexible and increasingly accessible technique. It can overcome significant challenges faced by researchers seeking to extend the capabilities of ultrafast sources, e.g. for attosecond science. Of particular interest is this method's ability to leverage both established and novel near-IR ultrafast lasers for the generation of novel ultrafast mid-IR sources. This promises exquisite control over the pulse shape down to single-cycle duration, as well as average-power and pulse energy scaling, all in the mid-IR. Additionally, this method could serve laser industry applications that benefit from its robustness and capability to transfer broad spectral bandwidth between spectral domains, e.g. to avoid angle tuning with multiple crystals, or perform broadband spectroscopy and imaging [90].

We hope that through this article we increase the familiarity of the ultrafast optics community in general, and the attosecond science community in particular, with adiabatic frequency conversion. There are strong indications that the introduction of this powerful technique into more venues of the ultrafast research and development landscape will facilitate new scientific and technological discoveries and achievements.

As evident by this review, adiabatic frequency conversion has been evolving since its first demonstration more than a decade ago. We expect this trend to continue, and that the very recent extension to FWM processes is a precursor to further exciting developments.

Acknowledgments

This publication is part of a project that has received funding from the European Research Council (ERC) under the European Union's Horizon 2020 Research and Innovation Programme (Grant Agreement No. 639402).

This work was supported by the US Dept. of Energy, Contract No. DE-SC0020141; US Office of Naval Research, Contract No. N00014-19-1-2592; US National Science Foundation, Contract No. ECCS-1944653.

ORCID iDs

Peleg Margules https://orcid.org/0000-0003-3557-3370
Jeffrey Moses https://orcid.org/0000-0002-2993-0100

References

[1] Corkum P and Krausz F 2007 Attosecond science *Nat. Phys.* **3** 381–7
[2] Krausz F and Ivanov M 2009 Attosecond physics *Rev. Mod. Phys.* **81** 163
[3] Gordon A and Kärtner F 2005 Scaling of keV HHG photon yield with drive wavelength *Opt. Express* **13** 2941–7
[4] Ivanov M, Yakovlev V and Krausz F 2008 Mid-infrared coherent sources and applications *NATO Science for Peace and Security Series B: Physics and Biophysics* ed M Ebrahim-Zadeh and I T Sorokina (Berlin: Springer) pp 589–98
[5] DiChiara A D, Ghimire S, Reis D, Dimauro L F and Agostini P 2013 Strong-field and attosecond physics with mid-infrared lasers *Springer Ser. Opt. Sci.* **177** 81–98
[6] Wolter B, Pullen M, Baudisch M, Sclafani M, Hemmer M, Senftleben A, Schröter C, Ullrich J, Moshammer R and Biegert J 2015 Strong-field physics with mid-IR fields *Phys. Rev.* X **5** 021034
[7] Baker S, Robinson J, Haroth C, Teng H, Smith R, Chirilă C, Lein M, Tisch J and Marangos J 2006 Probing proton dynamics in molecules on an attosecond time scale *Science* **312** 424–7
[8] Vozzi C *et al* 2010 High harmonic generation spectroscopy of hydrocarbons *Appl. Phys. Lett.* **97** 241103
[9] Popmintchev T *et al* 2012 Bright coherent ultrahigh harmonics in the keV x-ray regime from mid-infrared femtosecond lasers *Science* **336** 1287–91
[10] Popmintchev D *et al* 2015 Ultraviolet surprise: efficient soft x-ray high-harmonic generation in multiply ionized plasmas *Science* **350** 1225–31
[11] Fayer M D 2009 Dynamics of liquids, molecules, and proteins measured with ultrafast 2D IR vibrational echo chemical exchange spectroscopy *Annu. Rev. Phys. Chem.* **60** 21–38
[12] Först M, Manzoni C, Kaiser S, Tomioka Y, Tokura Y, Merlin R and Cavalleri A 2011 Nonlinear phononics as an ultrafast route to lattice control *Nat. Phys.* **7** 854–6

[13] Mehlenbacher R D, McDonough T J, Grechko M, Wu M, Arnold M S and Zanni M T 2015 Energy transfer pathways in semiconducting carbon nanotubes revealed using two-dimensional white-light spectroscopy *Nat. Commun.* **6** 6732
[14] Leone S *et al* 2014 What will it take to observe processes in 'real time'? *Nat. Photon.* **8** 162–6
[15] Wirth A *et al* 2011 Synthesized light transients *Science* **334** 195–200
[16] Huang S *et al* 2011 High-energy pulse synthesis with sub-cycle waveform control for strong-field physics *Nat. Photon.* **5** 475–9
[17] Manzoni C, Huang S-W, Cirmi G, Farinello P, Moses J, Kärtner F X and Cerullo G 2012 Coherent synthesis of ultra-broadband optical parametric amplifiers *Opt. Lett.* **37** 1880–2
[18] Boyd R W 2008 *Nonlinear Optics* 3rd edn, ed R W Boyd (New York, NY: Academic)
[19] Krogen P, Suchowski H, Liang H, Flemens N, Hong K, Kärtner F X and Moses J 2017 Generation and multi-octave shaping of mid-infrared intense single-cycle pulses *Nat. Photon.* **11** 222–6
[20] Levanon A, Dahan A, Nagler A, Lifshitz E, Bahar E, Mrejen M and Suchowski H 2017 Pulse shaping of broadband adiabatic SHG from a Ti-sapphire oscillator *Opt. Lett.* **42** 2992–5
[21] Suchowski H, Bruner B D, Arie A and Silberberg Y 2010 Broadband nonlinear frequency conversion *Opt. Photonics News* **21** 36–41
[22] Baudrier-Raybaut M, Haïdar R, Kupecek P, Lemasson P and Rosencher E 2004 Random quasi-phase-matching in bulk polycrystalline isotropic nonlinear materials *Nature* **432** 374–6
[23] Varon I, Porat G and Arie A 2011 Controlling the disorder properties of quadratic nonlinear photonic crystals *Opt. Lett.* **36** 3978–80
[24] Hum D S and Fejer M M 2007 Quashi-phasematching *C. R. Phys.* **8** 180–98
[25] Suhara T and Nishihara H 1990 Theoretical analysis of waveguide second-harmonic generation phase matched with uniform and chirped gratings *IEEE J. Quantum Electron.* **26** 1265–76
[26] Arbore M A, Galvanauskas A, Harter D, Chou M H and Fejer M M 1997 Engineerable compression of ultrashort pulses by use of second-harmonic generation in chirped-period-poled lithium niobate *Opt. Lett.* **22** 1341–3
[27] Suchowski H, Oron D, Arie A and Silberberg Y 2008 Geometrical representation of sum frequency generation and adiabatic frequency conversion *Phys. Rev.* A **78** 063821
[28] Suchowski H, Porat G and Arie A 2014 Adiabatic processes in frequency conversion *Laser Photonics Rev.* **8** 333–67
[29] Markov A *et al* 2018 Broadband and efficient adiabatic three-wave-mixing in a temperature-controlled bulk crystal *Opt. Express* **26** 4448–58
[30] Rozenberg E and Arie A 2019 Broadband and robust adiabatic second-harmonic generation by a temperature gradient in birefringently phase-matched lithium triborate crystal *Opt. Lett.* **44** 3358–61
[31] Liu X, Shen X, Rui T, He L, Zhou B and Zheng N 2020 Adiabatic nonlinear optical frequency conversion based on the electro-optic effect *Opt. Lett.* **45** 467–70
[32] Ding X, Habib S, Amezcua-Correa R and Moses J 2019 Near-octave intense mid-infrared by adiabatic down-conversion in hollow anti-resonant fiber *Opt. Lett.* **44** 1084–7
[33] Ding X, Heberle D, Harrington K, Flemens N, Chang W-Z, Birks T A and Moses J 2020 Observation of rapid adiabatic passage in optical four-wave mixing *Phys. Rev. Lett.* **24** 153902
[34] Liu X, Bruch A W, Lu J, Gong Z, Surya J B, Zhang L, Wang J, Yan J and Tang H X 2019 Beyond 100 THz-spanning ultraviolet frequency combs in a non-centrosymmetric crystalline waveguide *Nat. Commun.* **10** 2971
[35] Suchowski H, Prabhudesai V, Oron D, Arie A and Silberberg Y 2009 Robust adiabatic sum frequency conversion *Opt. Express* **17** 12731–40
[36] Suchowski H, Bruner B D, Ganany-Padowicz A, Juwiler I, Arie A and Silberberg Y 2011 Adiabatic frequency conversion of ultrafast pulses *Appl. Phys.* B **105** 697–702
[37] Moses J, Suchowski H and Kärtner F X 2012 Fully efficient adiabatic frequency conversion of broadband Ti: sapphire oscillator pulses *Opt. Lett.* **37** 1589–91
[38] Suchowski H, Krogen P R, Huang S, Kärtner F X and Moses J 2013 Octave-spanning coherent mid-IR generation via adiabatic difference frequency conversion *Opt. Express* **21** 28892–901
[39] Cankaya H, Calendron A, Suchowski H and Kärtner F X 2014 Highly efficient broadband sum-frequency generation in the visible wavelength range *Opt. Lett.* **39** 2912–5
[40] Phillips C R and Fejer M M 2010 Efficiency and phase of optical parametric amplification in chirped quasi-phase-matched gratings *Opt. Lett.* **35** 3093–5
[41] Phillips C R, Langrock C, Chang D, Lin Y W, Gallmann L and Fejer M M 2013 Apodization of chirped quasi-phasematching devices *J. Opt. Soc. Am.* B **30** 1551–68
[42] Heese C, Phillips C R, Gallmann L, Fejer M M and Keller U 2010 Ultrabroadband, highly flexible amplifier for ultrashort midinfrared laser pulses based on aperiodically poled Mg:$LiNbO_3$ *Opt. Lett.* **35** 2340–2
[43] Heese C, Phillips C R, Gallmann L, Fejer M M and Keller U 2012 Role of apodization in optical parametric amplifiers based on aperiodic quasi-phasematching gratings *Opt. Express* **20** 18066–71
[44] Heese C, Phillips C R, Mayer B W, Gallmann L, Fejer M M and Keller U 2012 75 MW few-cycle mid-infrared pulses from a collinear apodized APPLN-based OPCPA *Opt. Express* **20** 26888–94
[45] Mayer B W, Phillips C R, Gallmann L, Fejer M M and Keller U 2013 Sub-four-cycle laser pulses directly from a high-repetition-rate optical parametric chirped-pulse amplifier at 3.4 μm *Opt. Lett.* **38** 4265–8
[46] Mayer B W, Phillips C R, Gallmann L and Keller U 2014 Mid-infrared pulse generation via achromatic quasi-phase-matched OPCPA *Opt. Express* **22** 20798–808
[47] Bigler N, Pupeikis J, Hrisafov S, Gallmann L, Phillips C R and Keller U 2018 High-power OPCPA generating 1.7 cycle pulses at 2.5 μm *Opt. Express* **26** 26750–7
[48] Yaakobi O, Caspani L, Clerici M, Vidal F and Morandotti R 2013 Complete energy conversion by autoresonant three-wave mixing in nonuniform media *Opt. Express* **21** 1623–32
[49] Porat G and Arie A 2013 Efficient, broadband, and robust frequency conversion by fully nonlinear adiabatic three-wave mixing *J. Opt. Soc. Am.* B **30** 1342–51
[50] Lin Y W, Phillips C and Fejer M M 2015 Chirped quasi-phase-matching grating design for broad-bandwidth, engineerable-phase adiabatic second-harmonic generation *CLEO* SW1O.2
[51] Leshem A, Meshulam G, Porat G and Arie A 2016 Adiabatic second-harmonic generation *Opt. Lett.* **41** 1229–32
[52] Dahan A, Levanon A, Katz M and Suchowski H 2017 Ultrafast adiabatic second harmonic generation *J. Phys.: Condens. Matter* **29** 084004
[53] Lagatsky A A, Brown C T A, Sibbett W, Holmgren S J, Canalias C, Pasiskevicius V, Laurell F and Rafailov E U 2007 Efficient doubling of femtosecond pulses in aperiodically and periodically poled KTP crystals *Opt. Express* **15** 1155–60

[54] Bahar E, Ding X, Dahan A, Suchowski H and Moses J 2018 Adiabatic four-wave mixing frequency conversion *Opt. Express* **26** 25582–601
[55] Landau L D 1932 On the theory of transfer of energy at collisions II *Phys. Z. Sowjetunion* **2** 46–51
[56] Zener C 1932 Non-adiabatic crossing of energy levels *Proc. R. Soc.* A **137** 696–702
[57] Flemens N, Krogen P, Suchowski H, Liang H, Hong K, Kärtner F X and Moses J 2018 Single-cycle or arbitrarily shaped octave-spanning mid-infrared pulses: intrinsic and extrinsic pulse shaping in adiabatic frequency conversion *High-Brightness Sources and Light-driven Interactions, OSA Technical Digest (online) (Optical Society of America)* paper MW2C.7 (https://doi.org/10.1364/MICS.2018.MW2C.7)
[58] Goldstein H 1950 *Classical Mechanics* (Cambridge, MA: Addison-Wesley Press)
[59] Porat G, Suchowski H, Silberberg Y and Arie A 2010 Tunable upconverted optical parametric oscillator with intracavity adiabatic sum-frequency generation *Opt. Lett.* **35** 1590–2
[60] Porat G, Silberberg Y, Arie A and Suchowski H 2012 Two photon frequency conversion *Opt. Express* **20** 3613–9
[61] Porat G and Arie A 2012 Efficient two-process frequency conversion through a dark intermediate state *J. Opt. Soc. Am.* B **29** 2901–9
[62] Porat G and Arie A 2013 Efficient broadband frequency conversion via simultaneous adiabatic three wave mixing processes *Appl. Phys. Lett.* **102** 151108
[63] Zhou X, He S, Liu G, Zhao L, Yu L and Zhang W 2018 New developments in laser-based photoemission spectroscopy and its scientific applications: a key issues review *Rep. Prog. Phys.* **81** 062101
[64] Ullrich J, Moshammer R, Doron A, Schmidt L P H and Schmidt-Bocking H 2003 Recoil-ion and electron momentum spectroscopy: reaction-microscopes *Rep. Prog. Phys.* **66** 1463–545
[65] Jauregui C, Limpert J and Tünnermann A 2013 High-power fibre lasers *Nat. Photon.* **7** 861–7
[66] Zervas M N and Codemard C A 2014 High power fiber lasers: a review *IEEE J. Sel. Top. Quantum Electron.* **20** 219–41
[67] Müller M, Klenke A, Steinkopff A, Stark H, Tünnermann A and Limpert J 2018 3.5 kW coherently combined ultrafast fiber laser *Opt. Lett.* **43** 6037–40
[68] Saraceno C J, Sutter D, Metzger T and Ahmed M A 2019 The amazing progress of high-power ultrafast thin-disk lasers *J. Eur. Opt. Soc.* **15** 15
[69] Phillips C R, Mayer A S, Klenner A and Keller U 2015 Femtosecond mode locking based on adiabatic excitation of quadratic solitons *Optica* **2** 667–74
[70] Stegeman G I 1997 cascading: nonlinear phase shifts *Quantum Semiclass. Opt.* **9** 139–53
[71] Mayer A S, Phillips C R and Keller U 2017 Watt-level 10-gigahertz solid-state laser enabled by self-defocusing nonlinearities in an aperiodically poled crystal *Nat. Commun.* **8** 1673
[72] Tokita S, Hashida M, Masuno S, Namba S and Sakabe S 2008 0.3% energy stability, 100-millijoule-class, Ti: sapphire chirped-pulse eight-pass amplification system *Opt. Express* **16** 14875–81
[73] Nubbemeyer T *et al* 2017 1 kW, 200 mJ picosecond thin-disk laser system *Opt. Lett.* **42** 1381–4
[74] Lu C-H, Tsou Y-J, Chen H-Y, Chen B-H, Cheng Y-C, Yang S-D, Chen M-C, Hsu C-C and Kung A H 2014 Generation of intense supercontinuum in condensed media *Optica* **1** 400–6
[75] Jocher C, Eidam T, Hädrich S, Limpert J and Tünnermann A 2012 Sub 25 fs pulses from solid-core nonlinear compression stage at 250 W of average power *Opt. Lett.* **37** 4407–9
[76] Seidel M, Arisholm G, Brons J, Pervak J and Pronin O 2016 All solid-state spectral broadening: an average and peak power scalable method for compression of ultrashort pulses *Opt. Express* **24** 9412–28
[77] Keller U 2010 Femtosecond to attosecond optics *IEEE Photon. J.* **2** 225–8
[78] Krebs M, Hädrich S, Demmler S, Rothhardt J, Zaïr A, Chipperfield L, Limpert J and Tünnermann A 2013 Towards isolated attosecond pulses at megahertz repetition rates *Nat. Photon.* **7** 555–9
[79] Saule T *et al* 2019 High-flux ultrafast extreme-ultraviolet photoemission spectroscopy at 18.4 MHz pulse repetition rate *Nat. Commun.* **10** 458
[80] Witting T, Furch F, Osolodkov M, Schell F, Menoni C, Schulz C P and Vrakking M J J 2020 Generation and characterization of isolated attosecond pulses for coincidence spectroscopy at 100 kHz repetition rate *J. Phys. Conf. Ser.* **1412** 072031
[81] Nisoli M, Decleva P, Calegari F, Palacios A and Martín F 2017 Attosecond electron dynamics in molecules *Chem. Rev.* **117** 10760–825
[82] Chipperfield L E, Robinson J S, Tisch J W G and Marangos J P 2009 Ideal waveform to generate the maximum possible electron recollision energy for any given oscillation period *Phys. Rev. Lett.* **102** 063003
[83] Jin C, Wang G, Wei H, Le A-T and Lin C D 2014 Waveforms for optimal sub-keV high-order harmonics with synthesized two- or three-colour laser fields *Nat. Commun.* **5** 4003
[84] Haessler S *et al* 2014 Optimization of quantum trajectories driven by strong-field waveforms *Phys. Rev.* X **4** 021028
[85] Manzoni C, Mücke O D, Cirmi G, Fang S, Moses J, Huang S-W, Hong K-H, Cerullo G and Kärtner F X 2015 Coherent pulse synthesis: towards sub-cycle optical waveforms *Laser Photonics Rev.* **9** 129–71
[86] Batysta F *et al* 2016 Broadband OPCPA system with 11 mJ output at 1 kHz, compressible to 12 fs *Opt. Express* **24** 17843–8
[87] Liang H *et al* 2017 High-energy mid-infrared sub-cycle pulse synthesis from a parametric amplifier *Nat. Commun.* **8** 141
[88] You Y S *et al* 2017 Laser waveform control of extreme ultraviolet high harmonics from solids *Opt. Lett.* **42** 1816–9
[89] Riedel R *et al* 2014 Thermal properties of borate crystals for high power optical parametric chirped-pulse amplification *Opt. Express* **22** 17607–19
[90] Mrejen M, Erlich Y, Levanon A and Suchowski H 2020 Multicolor time-resolved upconversion imaging by adiabatic sum frequency conversion *Laser Photonics Rev.* **14** 2000040